La Niña, Climate change, high exposure and vulnerability combined led to devastating floods in parts of Southern Africa

Authors

Izidine Pinto, *Royal Netherlands Meteorological Institute (KNMI), De Bilt, The Netherlands*
Joyce Kimutai, *Centre for Environmental Policy, Imperial College, London, UK*
Mariam Zachariah, *Centre for Environmental Policy, Imperial College, London, UK*
Sjoukje Philip, *Royal Netherlands Meteorological Institute (KNMI), De Bilt, The Netherlands*
Arlindo Meque, *Independent researcher - Maputo, Mozambique*
Bernardino Nhantumbo, *Instituto Nacional de Meteorologia (INAM), Maputo, Mozambique*
Stefaan Conradie, *Climate System Analysis Group, University of Cape Town, Cape Town, South Africa*
Piotr Wolski, *Climate System Analysis Group, University of Cape Town, Cape Town, South Africa*
Renate Meyer, *Red Cross Red Crescent Climate Centre, The Hague, The Netherlands (based in Cape Town, South Africa)*
Maja Vahlberg, *Red Cross Red Crescent Climate Centre, The Hague, The Netherlands; Swedish Red Cross, Stockholm, Sweden (based in Ubmeje/Umeå, Sweden)*
Aynur Kadihasanoglu, *Red Cross Red Crescent Climate Centre, The Hague, The Netherlands (based in Geneva, Switzerland)*
Sojung Yoon, *Red Cross Red Crescent Climate Centre The Hague, The Netherlands (based in South Korea)*
Nick Baumgart, *Department of Public Health, Global Health Section and Copenhagen Centre for Disaster Research, University of Copenhagen*
Emmanuel Raju, *Department of Public Health, Global Health Section and Copenhagen Centre for Disaster Research, University of Copenhagen*
Gerbrand Koren, *Copernicus Institute of Sustainable Development, Utrecht University, Utrecht, The Netherlands*
Osvaldo Inlamea, *Instituto Nacional de Saúde (INS), Maputo, Mozambique*
Tatiana Marrufo, *Instituto Nacional de Saúde (INS), Maputo, Mozambique*
Plácida Maholela, *Instituto Nacional de Saúde (INS), Maputo, Mozambique*
Almiro Tivane, *Instituto Nacional de Saúde (INS), Maputo, Mozambique*
Américo José, *Instituto Nacional de Saúde (INS), Maputo, Mozambique*
Eduardo Samo Gudo, *Instituto Nacional de Saúde (INS), Maputo, Mozambique*
Friederike Otto, *Centre for Environmental Policy, Imperial College, London, UK London, London, UK*

Review authors

Ben Clarke, *Centre for Environmental Policy, Imperial College, London, UK*
Roop Singh, *Red Cross Red Crescent Climate Centre, The Hague, The Netherlands (based in New Jersey, USA)*
Dora Vrkić, *Grantham Institute - Climate Change and the Environment, Imperial College*

Cite as Pinto, I. et al., (2026): La Niña, Climate change, high exposure and vulnerability combined led to devastating floods in parts of Southern Africa (WWA scientific report No. 81) World Weather Attribution DOI: 10.25560/127388

Main findings

- The floods exposed deep and persistent social vulnerability in the region. Recurrent flooding and other natural hazards have trapped rural communities in the lower Limpopo River basin in a cycle of poverty. As a result, flood impacts are disproportionately severe for low-income and marginalized communities. A large proportion of the urban population living in conditions of informality, is particularly vulnerable to flooding, exacerbated by rapid urban expansion, inadequate planning, and insufficient provision of basic services. Poor housing quality and inadequate infrastructure significantly increase exposure and vulnerability to flooding.

- Historical mining practices, weak environmental regulation, and limited awareness of long-term impacts have entrenched persistent and severe damage to aquatic ecosystems which, in combination with long term low investment and low maintenance of aging infrastructure increased exposure dramatically.

- Flooding disproportionately harms vulnerable groups not simply through exposure, but by disrupting life-sustaining systems. Elderly people, persons with disabilities, and people living with HIV face heightened risks as floods damage health facilities, destroy medical supplies and cold-chain infrastructure, and cut off access to clinics, interrupting essential HIV and TB treatment and leading to long-term health complications beyond the flood event itself.

- Pre-existing food insecurity, driven by droughts and other hazards, will be sharply amplified by the floods affecting highly exposed agricultural communities in Mozambique and Eswatini.

- To estimate if human induced climate change influenced heavy rainfall over the region we first determine if there is a trend in observations in the heaviest 10-day rainfall. Although this event has an estimated return period of about 50 years and remains rare in today's climate, which has warmed by 1.3°C, it would have been much rarer in a climate 1.3°C cooler.

- In addition to climate change, extreme rainfall in this region is known to be influenced by ENSO. We find that the current phase of ENSO, a weak La Niña during the DJF season, increased the chances and severity of heavy rainfall. Our best estimates indicate that La Niña made such extreme 10-day precipitation more likely, by a factor of about 5 and increased 10-day intensity by about 22%. Thus, the effect of La Niña is about half as the effect of global warming.

- To assess to what extent the observed change can be attributed to human-induced climate change, we typically combine the observations with climate models. However, the models have limitations in this region and do not adequately capture the ENSO correlation. As a result, we cannot confidently attribute the *magnitude* of the observed change to climate change. However, we have confidence that climate change has increased both the likelihood and the intensity of the 10-day rainfall, based on the observed signal, physical understanding and existing literature.

- Flood policies exist across the region but are inconsistently implemented, limiting their effectiveness. Rapid urbanisation, resource constraints, and gaps in community-level preparedness leave many areas exposed to severe flooding. Strengthening flood resilience will require fully operationalising existing policies, as well as enhancing coordination across river basins, investing in local infrastructure and early warning systems, and building community capacity to prepare for, respond to, and recover from flood events.

- Compound hazards, such as when severe drought periods are interrupted by intense rainfall, cyclone or flooding events leave communities with low capacity to absorb the impact, or build coping strategies. Impacts from flooding such as livelihoods being disrupted - coupled with damage to homes and reduced access to healthcare - can also trigger a number of cascading risks such as disease outbreaks, critical system collapse and further displacement with heightened levels of inequity. Building community-level resilience to these compound and cascading risks is complex, requiring long-term, locally led adaptation that is also embedded within district, national, and regional strategies.

1 Introduction

Since 26 December 2025, Mozambique has experienced heavy rainfall that has triggered flooding across the provinces of Nampula, Niassa, Manica, Sofala, Tete, and Zambézia, affecting 75,325 people (14,310 families) (ReliefWeb, 2026). From 9 January, southern Zimbabwe, northeastern South Africa, and southern Mozambique experienced exceptionally heavy rainfall (Figure 1.1) and widespread flooding. Data from the National Institute of Meteorology (INAM) shows that several locations in Mozambique recorded record-breaking 24-hour rainfall totals, including 271.9mm on 11 January in Gaza (Massangena station), 213mm on 19 January in Maputo (Maputo Observatory), and 253mm on 10 January in Inhambane (Massinga station). Rainfall of 945mm was observed in parts of Limpopo (Tshanowa Primary in Greater Thohoyandou) over the event period, whereas the rainfall at Punda Maria (~575mm in 11 days from 9-19 Jan) and Shangoni (573mm) in the Kruger National Park in South Africa both substantially exceeded the mean annual rainfall at these stations (531 and 458mm, respectively) (SANPARKS, 2026).

Following heavy and persistent rains, rivers within the region exceeded their alert levels, causing large-scale flooding in South Africa, Mozambique, and Eswatini. Mozambique is particularly affected by heavy rains because its geographic position lies downstream of major regional river basins. Large-volume releases from upstream dams raise river levels, worsening and prolonging flooding in downstream areas. The event led to severe socioeconomic losses, characterized by loss of life, casualties, and extensive damage to critical infrastructure. For example, as of 21 January, the Government of Mozambique reported that over 600,000 people had already been affected by the event (OCHA, 2026), with the number expected to increase to at least 800,000 in the coming days due to the persistent rains and ongoing search and rescue efforts. Key impacts in Mozambique include extensive loss of lives (at least 18 people), infrastructure damage, with over 70,000 houses destroyed or flooded, 18 health facilities damaged, 10 schools partially or destroyed, and approximately 5,000 km of roads affected, including the main national road (N1), leaving the Gaza province cut off from the rest of the country. Additionally, the loss of over 105,000 hectares of land and 34,000 heads of livestock has severely undermined household livelihoods. Some of the regions currently experiencing floods are the same regions that endured an El Niño induced drought in the 2023/2024 rainy season (OCHA,2024).

These failed seasons worsened the conditions of the population since they have rainfed agriculture as their main source of livelihood.

A continental tropical low-pressure system, along with a mid-level easterly trough, formed around the central Mozambican coast on 6 January 2026. It gradually propagated south-westward to the Limpopo River basin, where it became trapped near the eastern escarpment of southern Africa, resulting in a stationary low-pressure system. The circulation to the south of the system was responsible for highly anomalous deep tropical moisture advection into the relatively dry subtropical coastal plains around the Lower Limpopo River valley. Intense moisture convergence along these coastal plains—and later (from about 12 January) convergence against the steep slopes of the eastern escarpment of Limpopo and Mpumalanga—led to persistent heavy rainfall (Figure 1.1). From the 18th of January, an upper-tropospheric westerly wave trough moved across South Africa. A pronounced tropical temperate trough (TTT) developed ahead of the upper-trough, which interacted with the tropical low from the evening of the 18th. This extended the period of heavy rainfall, but the low was eventually displaced into the Mozambican Channel on the 20th of January by the westerly trough.

Synoptic-Scale tropical continental lows over southern Africa can occur from December to March and have been termed Africánes (Viljoen et al, 2022). The interior parts of the lower Limpopo basin are the preferred location for such systems below 20°S, but on average, this region sees only 1 or 2 events per season, which still contribute around 30% of the seasonal rainfall totals (Viljoen et al, 2022). Africánes have been known to cause extreme rainfall and flooding in South Africa in combination with TTTs (Viljoen et al., 2022). Further focused analysis would be required to establish whether this system satisfies all conditions for an Africáne, but it exhibits substantial similarities with the phenomenon.

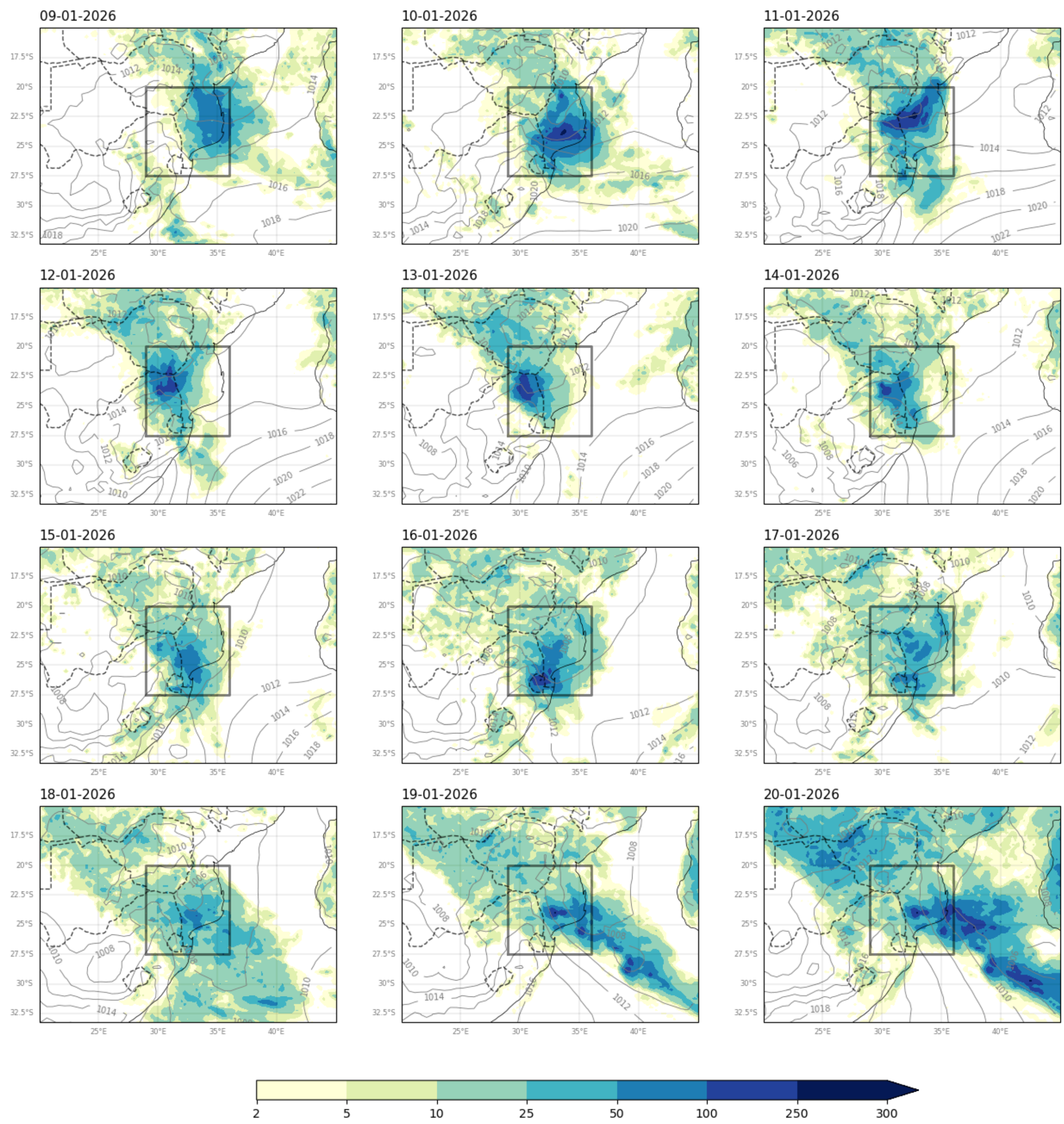

Figure 1.1: *Daily rainfall (color scale, in mm) and mean sea level pressure (contour lines, in hPa) between 09-20 January 2026. The study region is highlighted in black. Data ERA5 analysis and forecast.*

1.1 Extreme rainfall in East Southern Africa

The 2026 floods are the third event of comparable magnitude to strike the same region in less than 30 years, highlighting a recurring pattern following the floods of February 2000 (Reason and Keibel, 2004) and January 2013 (Manhique et al., 2015). The floods in 2000 were caused by a combination of a tropical depression that occurred in early February and the tropical cyclone Eline, which occurred in late February when the soil was already saturated. The 2000 floods resulted in at least 800 fatalities in

Mozambique and widespread damage to public and private infrastructure, crop and livestock losses. The January 2013 floods, the second floods of similar magnitude, impacted central and southern Mozambique, causing at least 100 fatalities, displacements of at least 200,000 people, destruction of infrastructures, and disruption of livelihoods (Manhique et al., 2015). The 2013 catastrophic flooding was associated with an active South Indian Convergence Zone (SICZ), maintained by a persistent low-level atmospheric trough (Manhique et al., 2015). `

Historical trends are known to be spatially inhomogeneous and strongly depend on the type of data used, period analysis and type of climate models used (Rouault et al., 2024; Tim et al., 2023). Summarising the available evidence for Eastern Southern Africa, working group 1 of the sixth assessment report (AR6) of the IPCC found that there has been an intensification of heavy precipitation in the region to date, but that there was low confidence in the attribution of this trend to anthropogenic influence (Masson-Delmotte et al., 2021). Since this report, several attribution studies have been undertaken for a diversity of extreme rainfall events in the region (McBride et al., 2022; Mpungose et al., 2022; Tim et al., 2023; Engelbrecht et al., 2025). For instance, Cyclone Ana brought heavy rainfall to Mozambique, Zimbabwe, Malawi and Madagascar. Despite challenges around the availability of observational data and climate model fidelity, the evidence suggested that climate change amplified the rainfall from this storm (Otto et al., 2022). In April 2022, heavy rainfall in parts of eastern South Africa was approximately doubled in likelihood, or equivalently made 4-8% more intense, by the influence of global warming (Pinto et al., 2022). Finally, in February 2025, parts of Botswana and South Africa experienced heavy rainfall that was found to be strongly increasing with warming, though again global and regional climate models did not capture this trend (Clarke et al., 2025). The consistency in increasing trends in extreme rainfall across different subregions, rainfall durations, and seasons suggests that confidence is now higher than in AR6 that climate change is influencing such events. However, the range of extreme rainfall driving mechanisms in the region, the uniqueness of the current event, and challenges around model capabilities mean that further study is required, using both probabilistic and other attribution approaches.

1.2 Event Definition

To capture the range of impacts from the persistent heavy rainfall affecting Mozambique, South Africa, Eswatini, and Zimbabwe (27.5–20°S, 29–6°E - ESAf; land only over the bounding box in Fig. 1.2), we analyse 10-day maximum rainfall accumulations (Rx10day) during the December–February (DJF) season. The Rx10day are calculated using only land-based data points.

This season was selected because it represents the primary rainfall period in the region, during which the dominant rainfall-generating mechanisms are similar, including the influence of ENSO. For the spatial domain, we focus on a climatologically homogeneous region partially encompassing the major river catchments (Limpopo, Umbeluzi, Maputo, Incomati, Save and Buzi) and the most affected surrounding areas. Figure 1.2 (right) shows the percentage contribution of the wettest 10-day rainfall period to the climatological DJF (1991-2020) total rainfall. During the event, large parts of the region experienced accumulated rainfall exceeding 400 mm over a 10-day period. A pronounced core of positive anomalies is centered over the interior of the domain, where the 10-day rainfall accounts for approximately 40–80% (and locally more) of the typical DJF total.

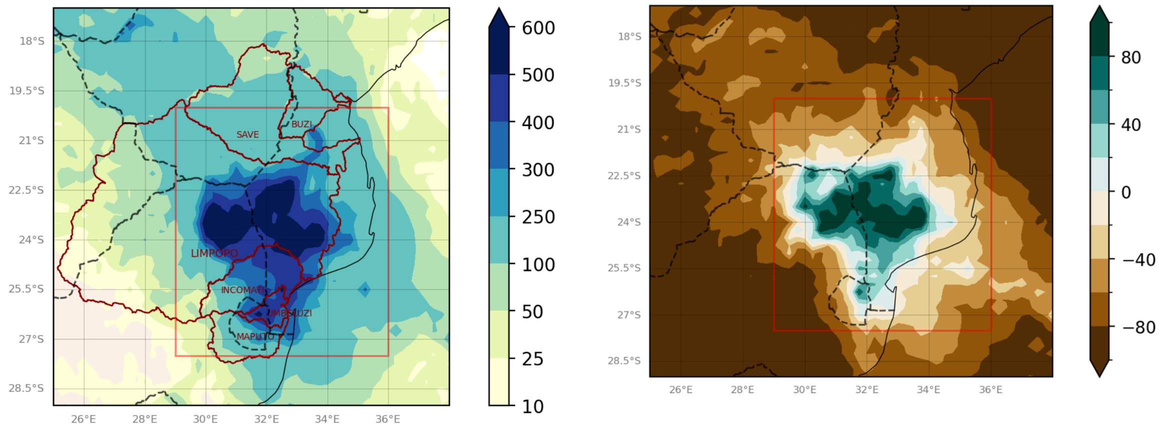

Figure 1.2: *Accumulated rainfall over parts of Mozambique, South Africa, Eswatini and Zimbabwe (ESAf) from 10-19 January 2025 (Left). The orange square indicates the study region (land only), black dashed lines are the country borders, and the red shapes indicate the catchment areas for which the names are included in the figure. Event rainfall expressed as a percentage of the mean DJF total rainfall (1991-2020) (right). Data from ERA5.*

In this report, we study the influence of anthropogenic climate change by comparing the likelihood and intensity of similar rainfall extremes at present with those in a 1.3°C cooler climate. We also extend this analysis into the future by assessing the influence of a further 1.3°C of global warming from present. This is in line with the latest Emissions Gap Report from the United Nations Environment Programme, which shows that the world is on track for at least 2.6°C temperature rise given currently implemented policies (UNEP, 2024).

2 Observed trends

2.1 Trends in gridded data

In this section, five gridded datasets (Section A1) are used to estimate the return period of the observed event in the current climate and to assess changes in the likelihood of such an event associated with an observed global mean surface temperature (GMST) warming of 1.3°C. Prior to the analysis, the datasets are compared (Fig. 1.3). The datasets differ in record length (Section A1) and exhibit substantial variability, suggesting a potential role of dynamical factors in driving extremes in the study region. However, during the common analysis period, there is strong agreement among the datasets in the timing of high and low rainfall periods, but with CHIRPS being generally higher. The 2026 event is well captured in the ERA5, CPC, and MSWEP datasets, with the exception of TAMSAT, which shows a lower magnitude. In the ERA5, CPC, and MSWEP datasets, the 2026 Rx10day event far exceeds the magnitude of any event previously recorded in these datasets.

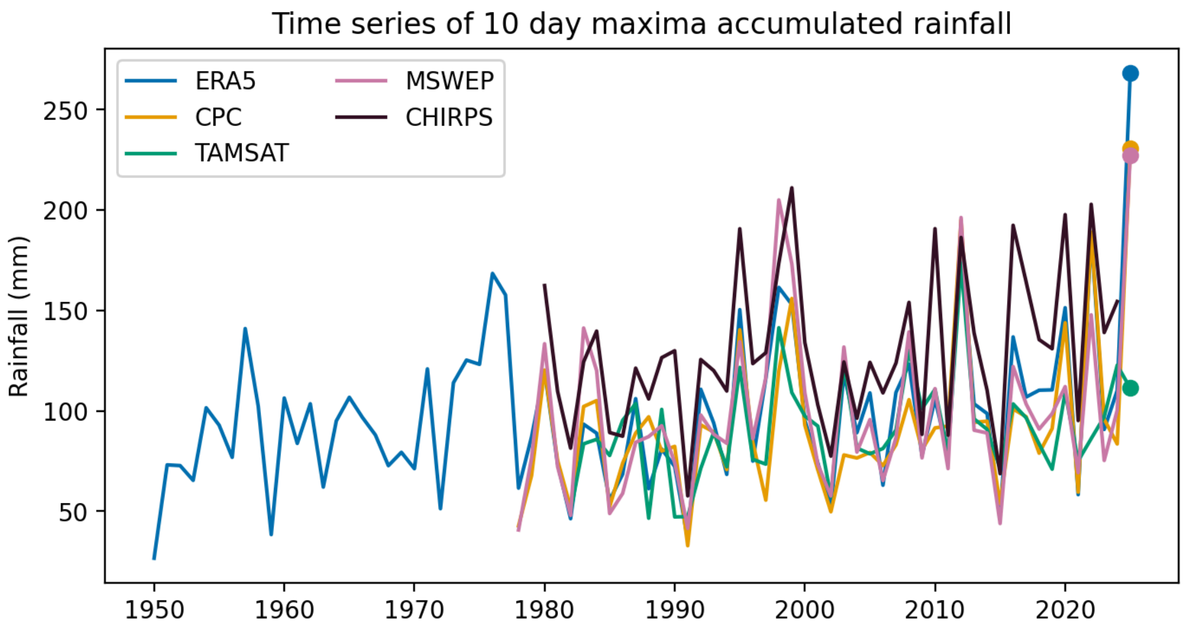

Figure 1.3: *10-day accumulated rainfall over study area for ERA5, CPC, TAMSAT, MSWEP and CHIRPS.*

Below, we explore two complementary statistical modeling approaches to assess potential drivers of changes in extreme rainfall in the region. First, we fit a non-stationary GEV distribution in which precipitation scales exponentially with global mean surface temperature (GMST). Second, we fit a nonstationary GEV distribution in which precipitation scales exponentially with both GMST and the detrended Niño3.4 index (see Section A1.3).

2.1.1. Influence of human-caused warming

The left-hand panels of Fig. 1.4 shows annual Rx10day as a function of GMST alone. The observed 2026 maximum in each dataset (pink markers) is included in the trend fitting. The dashed green line denotes a nonparametric LOESS fit; across all datasets, this indicates an increasing trend in Rx10day over the ESAf region. The right-hand panels in Figure 3.2 show the return period curves for the current (2026) climate and a 1.3°C cooler climate representing a pre-industrial world. All datasets show increasing trends in the likelihood and intensity of Rx10day events in the region because of both warming (GMST).

Table 2.1 summarises the return periods, magnitude of the 10-day rainfall during 9 June-19 January 2026 in the study domain. The event has a long return period in CPC, MSWEP, ERA5, and CHIRPS. To test the effect of the shorter ERA5 record, we refit the model using ERA5 data starting in 1979 and found a return period of approximately 59 years (95% CI: 12.3 to ∞), which is not substantially different from the estimates from the other datasets. In contrast, TAMSAT yields a much shorter return period of about 2 years, likely because the event magnitude in TAMSAT is less than half that observed in the other datasets.

All observational datasets agree on the order of magnitude of the trend towards increased precipitation totals, with best estimates for intensity change ranging from 44% to 74%, and best estimates in probability ratio ranging between 7 and almost infinity, which means such an event was very unlikely to happen in the past.

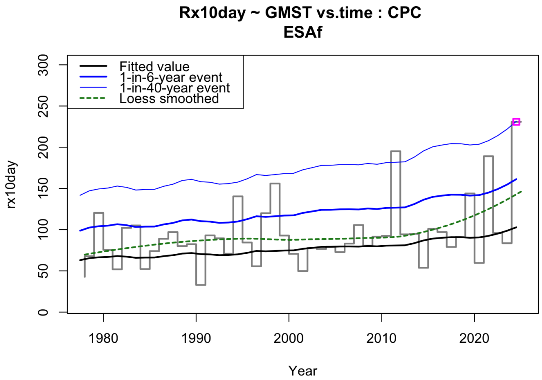

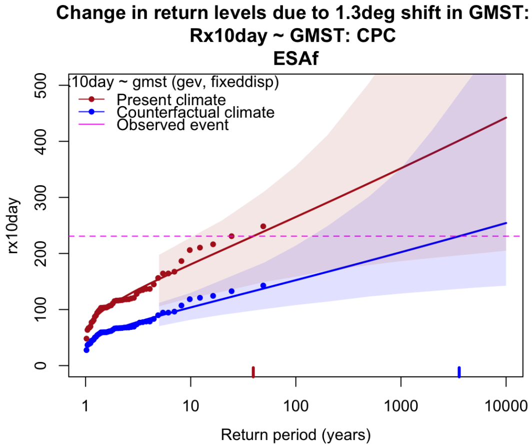

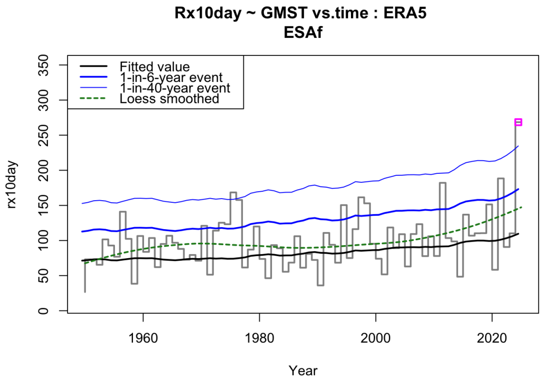

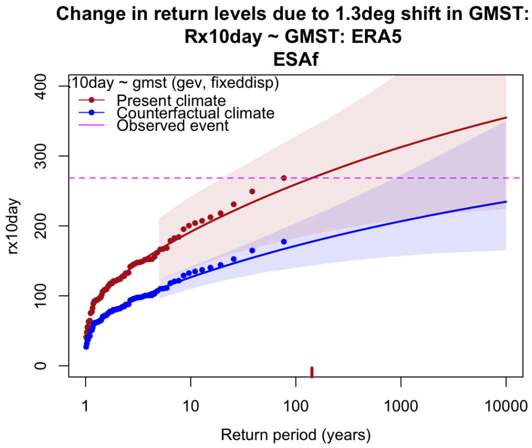

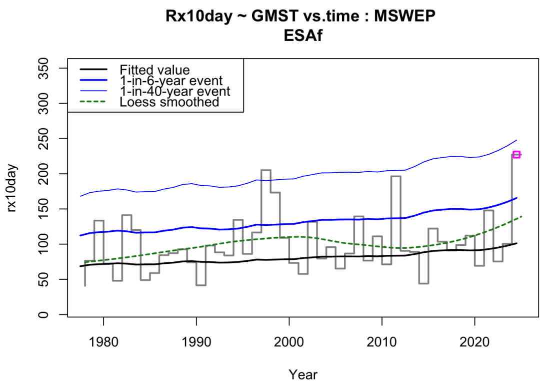

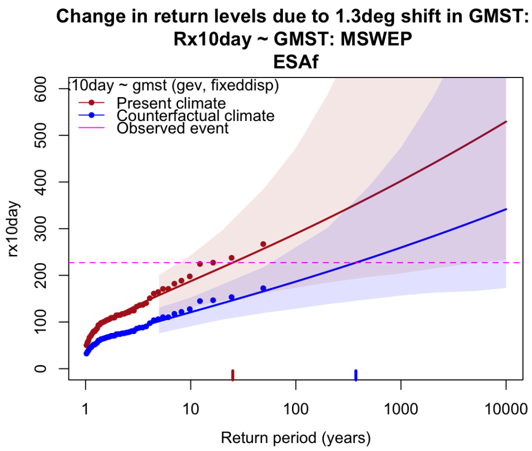

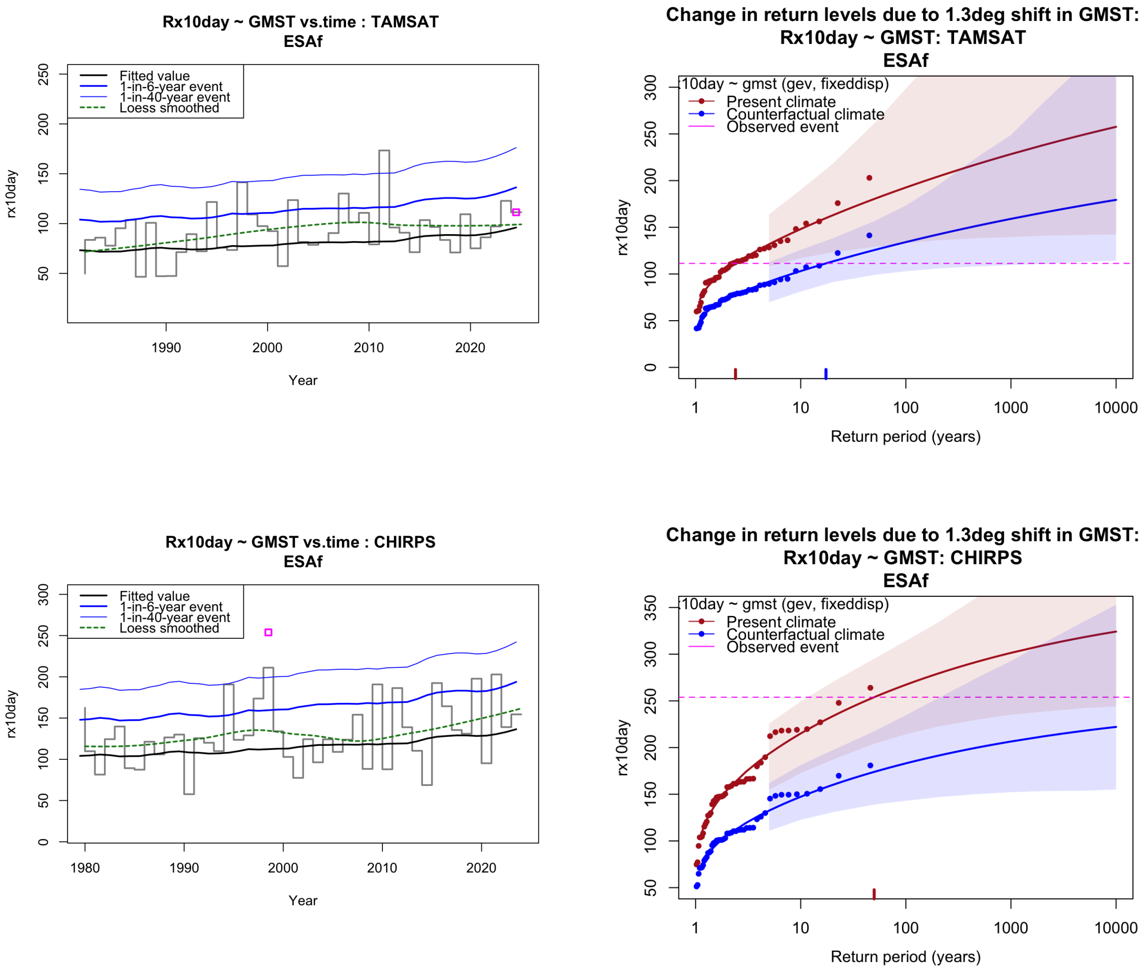

Figure 1.4: *GEV fit with fixed dispersion parameter scaling proportional to GMST. (**Left**) observed DJF Rx10day [mm/10day] as a function of the smoothed GMST. The solid black line shows the fitted trend associated with increasing GMST. The 2026 observation is highlighted with the magenta box, except for CHIRPS. (**Right**) return time plots for the climate of 2026 (red) and a climate with GMST 1.3ºC cooler (blue). The past observations are shown twice: once shifted up to the current climate and once shifted down to the climate of the pre-industrial era. The markers show the data and the lines show the expected return levels, with shading showing a bootstrapped 95% confidence interval. The magenta line shows the magnitude of the 2025 event analysed here. Results are shown for CPC (**top**), ERA5 (**second row**), MSWEP (**third row**), TAMSAT (**fourth row**) and CHIRPS (**bottom**).*

Table 2.1*: Estimated return periods of Rx10day over the study region in each observational data product, along with the respective changes in probability ratio and magnitudes associated with 1.3°C of global warming. Numbers in brackets are 95% confidence intervals obtained by bootstrapping. No confidence interval is given for the return period in CHIRPS because the data did not cover the event at the time of writing, so the return period was fixed at 50 years*

Dataset	Rx10day			
	Magnitude (mm/10day)	Return period (95% C.I.)	Change in intensity (%)	Probability Ratio
CPC	230.8	39 (11 to 7.6e+5)	74 (6.8 to 1.7e+2)	90 (1.8 to 1.1e+7)

ERA5	268.5	140 (20 to ∞)	51 (8.3 to 1.1e+2)	3060 (3.4 to ∞)
MSWEP	227.2	25 (7.7 to 5.5e+3)	55 (-2.6 to 1.6e+2)	15 (0.8 to ∞)
TAMSAT	111.3	2.4 (1.5 to 6.2)	44 (0.31 to 1.3e+2)	7.3 (1.0 to 1240)
CHIRPS	253.9	50	46 (3.4 to 96)	2e+11 (1.3 to ∞)

2.1.2 Influence of modes of natural variability

Tropical and subtropical teleconnections, most notably the El Niño–Southern Oscillation (ENSO) are major drivers of rainfall variability across sub-Saharan Africa (Camberlin et al., 2001). During the austral summer (November–April), La Niña conditions promote positive rainfall anomalies over southern Africa, including the study area, by modulating the position and intensity of large-scale circulation systems responsible for synoptic rainfall processes. These systems include the South Indian Convergence Zone (SICZ; Hoell et al., 2015; Hart et al., 2018) and the Intertropical Convergence Zone (ITCZ; Schneider et al., 2014).

El Niño years, which are characterized by warmer sea surface temperatures within the equatorial eastern Pacific Ocean, tend to favor widespread dry conditions within the study region. This is due to the disruption of the onshore moisture flux from the Indian Ocean and weakening of the Angola Low (Pomposi et al., 2018). Some of the observed multi-year droughts (e.g., mid 1980s, the 2014-2016 protracted drought) have been linked to El Niño conditions (Archer et al., 2017; Hoell et al., 2023). On the other hand, cooler temperatures in the Pacific Ocean, generally observed during the La Niña years, tend to produce above-normal rainfall conditions over Southern Africa (Rouault et al., 2024).

Given that ENSO modulates rainfall variability in the region, the nonstationary model is extended to incorporate ENSO as an additional covariate (Section A1.3). ENSO is represented by the relative Niño3.4 index, averaged over the October-December period. Fitting a statistical model using both GMST and this ENSO index as covariates gives an improved fit, according to the AIC, than GMST alone. ENSO was found to be important to explain the variability in the observed precipitation, consistent with previous research. Most previous heavy precipitation events in the area occurred during La Niña years and similarly the role of La Niña in this event was significant. In observations, compared to a neutral ENSO phase, the current (December-February) La Niña resulted in a consistent increase across all datasets, indicating its importance in the analysis.

Figure 1.4 shows annual Rx10day as a function of GMST and ENSO. The statistical model indicates that Rx10day is influenced by both long-term global warming, represented by GMST, and interannual climate variability associated with ENSO. All datasets show increasing trends in the likelihood and intensity of Rx10day events in the region because of both warming (GMST) and El Niño conditions.

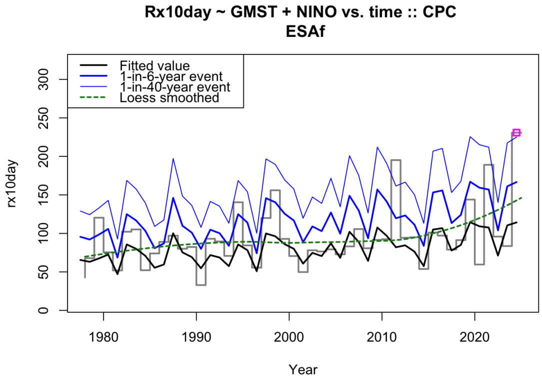

Rx10day ~ GMST + NINO vs. time :: CPC
ESAf
Fitted value
1-in-6-year event
1-in-40-year event
Loess smoothed
rx10day
Year

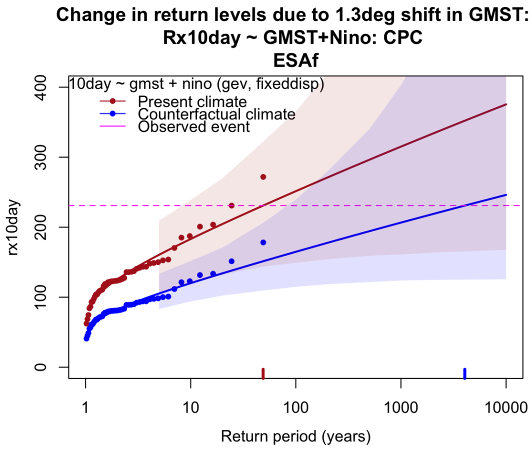

Change in return levels due to 1.3deg shift in GMST:
Rx10day ~ GMST+Nino: CPC
ESAf
10day ~ gmst + nino (gev, fixeddisp)
Present climate
Counterfactual climate
Observed event
rx10day
Return period (years)

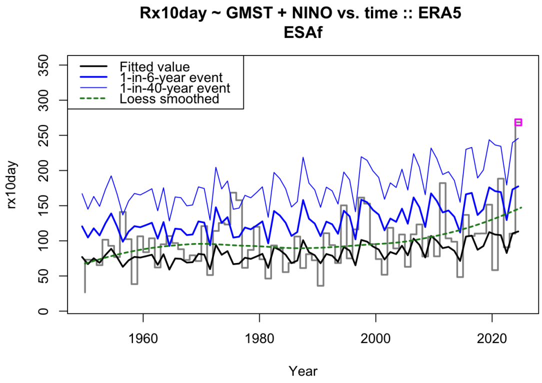

Rx10day ~ GMST + NINO vs. time :: ERA5
ESAf
Fitted value
1-in-6-year event
1-in-40-year event
Loess smoothed
rx10day
Year

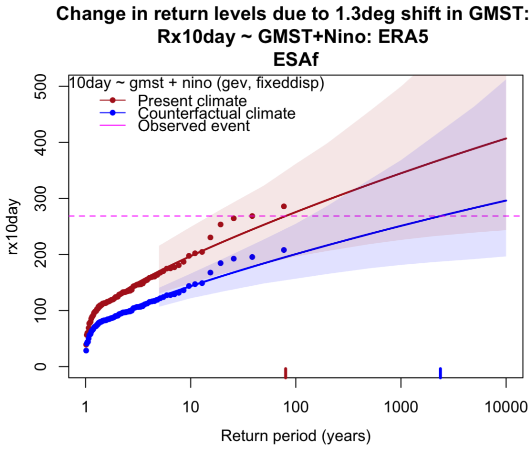

Change in return levels due to 1.3deg shift in GMST:
Rx10day ~ GMST+Nino: ERA5
ESAf
10day ~ gmst + nino (gev, fixeddisp)
Present climate
Counterfactual climate
Observed event
rx10day
Return period (years)

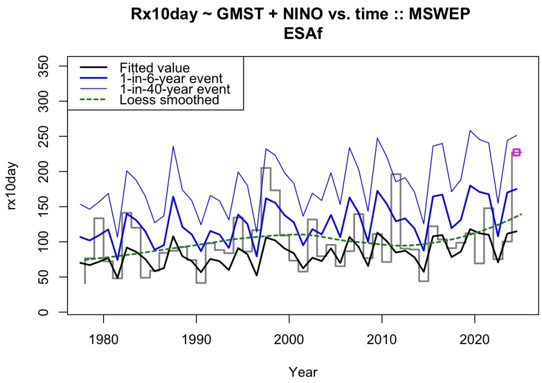

Rx10day ~ GMST + NINO vs. time :: MSWEP
ESAf
Fitted value
1-in-6-year event
1-in-40-year event
Loess smoothed
rx10day
Year

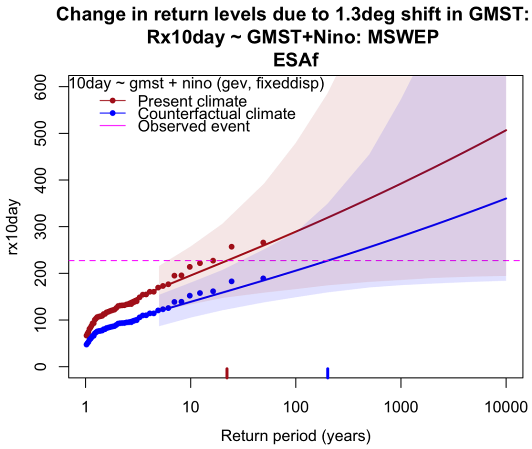

Change in return levels due to 1.3deg shift in GMST:
Rx10day ~ GMST+Nino: MSWEP
ESAf
10day ~ gmst + nino (gev, fixeddisp)
Present climate
Counterfactual climate
Observed event
rx10day
Return period (years)

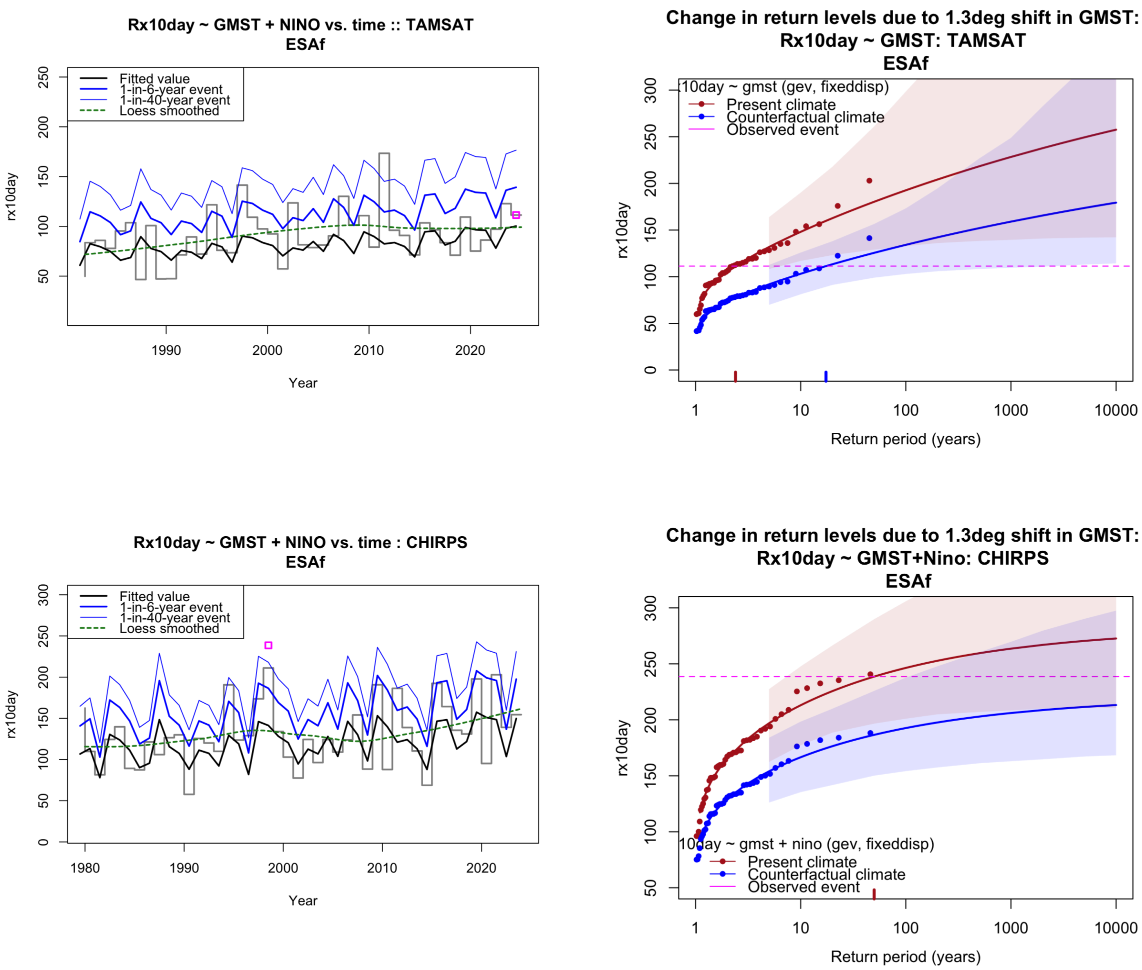

Figure 1.5: *Same as figure 1.4 but including both GMST and ENSO as covariates.*

Table 2.2 presents the return periods, magnitudes, and probability ratios of Rx10day derived from a statistical model incorporating both GMST and ENSO. Overall, the estimated return periods are comparable to those from the GMST-only model, with the exception of ERA5, for which the return period is around 80 years.

In the observational datasets, relative to a climate that is 1.3°C cooler, the statistical model incorporating both GMST and ENSO indicates an increase in intensity ranging from 31.9% to 52% across datasets. Relative to an ENSO-neutral state, the current La Niña conditions are associated with an intensity increase of 13.2% to 29.4% across the different observational datasets (Table 2.2). The fitted model indicates that ENSO explains much of the interannual variability in Rx10day, while rising global mean surface temperature drives a systematic increase in both typical and rare multi-day rainfall extremes. Consequently, ENSO-related events now occur on a warmer, wetter background climate, leading to substantially amplified extremes.

Since the statistical model is better, we communicate the observational results for the GMST+ENSO fits. To maintain statistical robustness given the relatively short observational records (mostly spanning ~1979 to the present), we adopt a 1-in-50-year event based on the range of datasets. This selection does not influence the estimated changes in magnitude and yields a slightly lower, more tightly constrained probability ratio than would be obtained for rarer events. Moreover, the 50-year return period is also used as a standard benchmark in risk assessment.

Table 2.2: *Change in probability ratio and magnitude for Rx10day in ESAf region due to both GMST and ENSO.*

Dataset	Event		GMST		ENSO	
	Magnitude (mm)	Return period (95% C.I.)	Probability Ratio	Change in magnitude (%)	Probability Ratio	Change in magnitude (%)
CPC	230.8	49 (8 to ∞)	82 (0.36 to ∞)	52 (-9.9 to 139)	9.6 (2.16 to ∞)	27.6 (16 to 42)
ERA5	268.5	80 (15 to 9.4e+6)	29.7 (1.24 to ∞)	37 (2.35 to 87)	4.5 (1.43 to ∞)	17.3 (3.8 to 33.6)
MSWEP	227.2	22 (6 to ∞)	9 (0.23 to ∞)	40.6 (-14.7 to 126)	5 (1.8 to ∞)	29.4 (14.3 to 50.5)
TAMSAT	111.3	2 (1.3 to 5.8)	3.9 (0.6 to 61.8)	31.9 (-6.9 to 90.4)	1.6 (1.1 to 10.8)	13.2 (1.9 to 25.4)
CHIRPS	253.9	50	9.4e+6 (0.14 to ∞)	27.9 (-1.5 to 75)	864 (5.1 to ∞)	23.3 (12.4 to 37.1)

3 Attribution of trends

3.1 Evaluation of climate models

In the subsections below, we show the results of the model evaluation for each location. The climate models are evaluated against the observations in their ability to capture:

1. **Seasonal cycles**: For this, we qualitatively compare the seasonal cycles based on model outputs against observations-based cycles. We discard the models that exhibit ill-defined peaks in their seasonal cycles. We also discard the model if the rainy season onset/termination varies significantly from the observations.
2. **Spatial patterns**: Models that do not match the observations in terms of the large-scale precipitation patterns are excluded.
3. Parameters of the fitted statistical models. We discard the model if the model and observation parameters ranges do not overlap.

In this study, however, none of the available models were able to satisfactorily reproduce the observed correlations with ENSO in the region — the role of La Niña conditions in enhancing rainfall. Nearly all CORDEX models also failed to reproduce the observed spatial climatological patterns. HIGHRESMIP models exhibit the large discrepancy with observed statistical parameters. Therefore, instead of a full evaluation, we adopt a stringent filtering approach, discarding those models that clearly exhibit uncertainties in the statistical parameters and fail to capture the spatial patterns.

The models are labelled as ‘good’,’reasonable’, or ’bad’ based on their performances in terms of the three criteria discussed above. A model is given an overall rating of ‘good’ if it is rated ‘good’ for all three characteristics. If there is at least one ‘reasonable’, then its overall rating will be ‘reasonable’ and ‘bad’ if there is at least one ‘bad’. For each framing or model setup we also use models that only just pass the evaluation tests with one label 'reasonable since we have less than five models that perform well. Overall, 8 of the CORDEX models and 2 HIGHRESMIP models were retained in this study. Tables of the model evaluation results can be found in Appendix A1.

3.2 Synthesis of results

For the two rainfall event definitions over the study region described above, we evaluate the influence of anthropogenic climate change on the events as observed in 2026 by calculating the probability ratio as well as the change in intensity using observations and climate models. Models which do not pass the evaluation described above are excluded from the analysis. The aim is to synthesise results from models that pass the evaluation along with the observations-based products, to give an overarching attribution statement.

Figures 3.1 show the changes in intensity for the observations (blue). Before combining them into a synthesised assessment, first, a representation error is added (in quadrature) to the observations, to account for the difference between observations-based datasets that cannot be explained by natural variability. This is shown in these figures as white boxes around the light blue bars. The dark blue bar shows the average over the observation-based products. Next, a term to account for intermodel spread is added (in quadrature) to the natural variability of the models. This is shown in the figures as white boxes around the light red bars. The dark red bar shows the model average, consisting of a weighted mean using the (uncorrelated) uncertainties due to natural variability plus the term representing intermodel spread (i.e., the inverse square of the white bars).

Observation-based products and models are combined into a single result in two ways. Firstly, we neglect common model uncertainties beyond the inter-model spread that is depicted by the model average, and compute the weighted average of models (dark red bar) and observations (dark blue bar): this is indicated by the magenta bar. As, due to common model uncertainties, model uncertainty can be larger than the inter-model spread, secondly, we also show the more conservative estimate of an unweighted, direct average of observations (dark blue bar) and models (dark red bar) contributing 50% each, indicated by the white box around the magenta bar in the synthesis figures.

All five observational datasets clearly show trends towards more rainfall in Rx10day in the study region. As shown in Section 2.1.2, the best estimates of the intensity change associated with global warming range from about 38% (-8%,107%) when using the full statistical model that includes GMST together with ENSO as covariates. As shown in Section 2.3.1, the simplified GMST-only model produces similar results, with an estimated change of 54% (0.44%, 107%), indicating that although including ENSO explains more of the year-to-year variability and reduces the trend associated with GMST, it does qualitatively affect the long-term trend driven by GMST. The contribution from ENSO (La Niña conditions observed during the event, in this case) is found to have added about 22% (5%, 44%) more rainfall as compared to neutral Niño conditions and 5 (0.9,149) times more likely. Due to the climate models evaluated for this study region not reliably reproducing the observed spatial climatological patterns (Section A2) or the rainfall–ENSO correlations (not shown), even the ones that evaluate better (2 out of the 3 criteria; see Table A3.1) are not consistent in the direction of change (Fig. 3.2). Therefore, we do not combine them with the observations for a formal attribution. Figure 3.2 compares changes in intensity from observations (blue) and models (red), showing that the models fail to reproduce the intensity changes observed in the data. Regional and global climate models are known to have limited ability to resolve deep convection associated with meso-scale weather systems such as subtropical lows, squall lines, and tropical cyclones that are characteristic of this region, and this may in part be responsible for the inconsistencies (e.g., [Prein et al., 2015](); [Lucas-Picher et al., 2021]()).

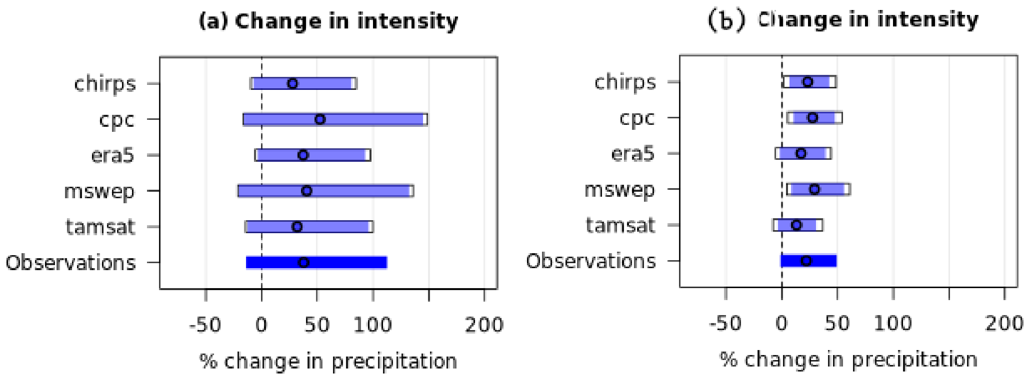

Figure 3.1 *Changes in Intensity of Rx10day over the region based on observation associated with (a) 1.3°C of global warming using the full statistical model that includes both GMST and ENSO as covariates (b) prevailing ENSO conditions using a statistical model that uses ENSO only as covariate i.e La Nina vs neutral conditions .*

The synthesised observations indicate a trend of about 40% which is 4 times more than the 10% increase due to 1.3°C of warming until now, expected from the Clausius-Clayperon relationship. Based on the observed signal, physical understanding and existing literature, we have confidence that climate change has increased both the likelihood and the intensity of Rx10day rainfall in the region. We conclude that an increasing trend in rainfall in observations is expected due the contribution from the Clausius-Clayperon relation that prescribes that a warmer atmosphere can hold more moisture and thus lead to more precipitation. However, the observed increase is much larger than expected from Clausius-Clayperon suggesting additional changes in the atmospheric dynamics contribute to the observed trend. Since the climate models do not simulate the dynamics well, we do not provide a synthesised statement of the role of anthropogenic climate change, as we cannot adequately quantify the role of climate change with the available models.

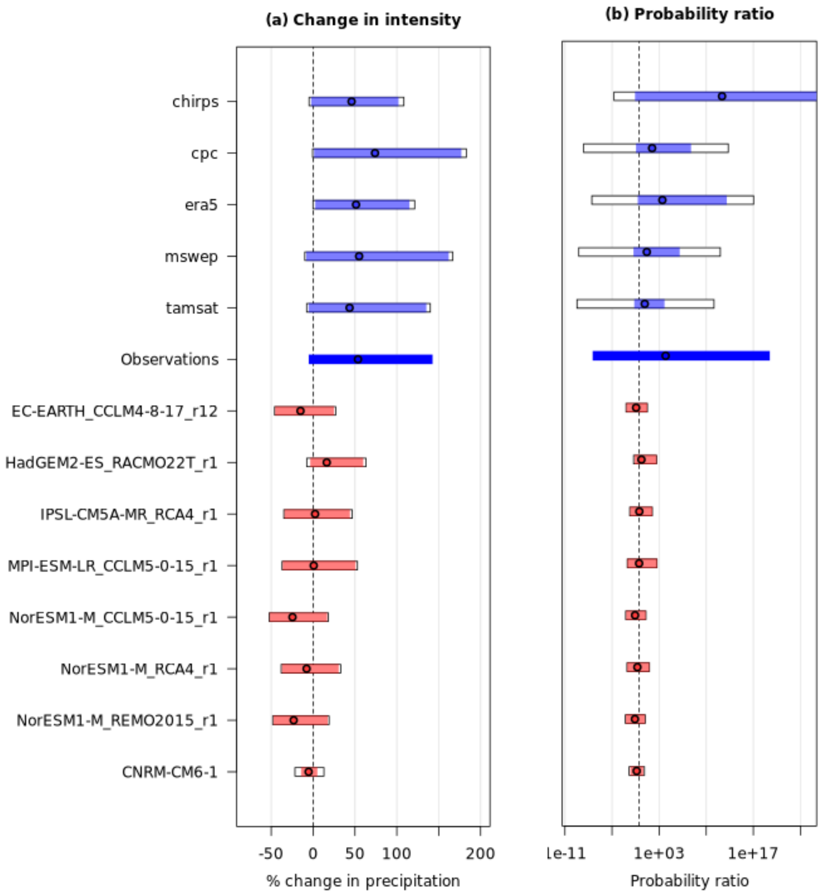

Figure 3.2 (a) Change in intensity for Rx10day over the study region in % from past to present (b) same as (a) for Probability Ratio (PR). Note that we do not combine the models or perform a full synthesis including observations and the models, and therefore excluded from this illustration.

4 Vulnerability and exposure

Since late December 2025, persistent rainfall has generated widespread flooding across southern Mozambique, eastern South Africa, Eswatini, and eastern Zimbabwe, with conditions intensifying in mid-January (ECHO, 2026). Multi-day precipitation totals exceeding seasonal norms triggered riverine flooding, flash floods, and emergency dam releases across the transboundary Limpopo and Zambezi basins (Republic of South Africa, 2026). The event has been characterized by slow-onset inundation in major floodplains alongside sudden surges in tributaries, resulting in hundreds of fatalities, large-scale displacement, and prolonged disruption across rural and urban areas (CCCM Cluster & IOM, 2026; Sky News, 2026; Al Jazeera, 2026).

Flood severity reflects the interaction between extreme rainfall and the region's topographic and hydrologic setting. Extensive low-lying coastal plains and interior river valleys, often below 100m elevation, paired with channels and drainage networks, concentrate upstream runoff into constrained outlets (Lourenco Saveca et al., 2022; Odiyo et al., 2019; SADC, 2018). These dynamics are amplified where settlements, agriculture, and infrastructure occupy historical floodplains. While many losses and damages are being reported, it is important to note, many impacts are potentially invisible such as losses in cultural heritage, social cohesion, agency, and overall wellbeing (Boyd et al, 2021).

In Mozambique, to date, approximately 594,681 people have been affected across 111,937 households, and 40% of the Gaza province was underwater (DW, 2026). In the province capital, Xai-Xai, many streets are recorded as being under water and authorities have called for full evacuation of low-lying neighbourhoods, issued alerts for downtown areas, and warned of crocodiles entering flooded streets (UN News, 2026). Large numbers of residents are sheltering in schools, churches and public buildings, reflecting both high exposure of central districts and limited formal evacuation infrastructure. Maputo city and other provincial capitals (e.g. in Inhambane, Sofala, Zambézia) have seen widespread flooding of houses, classrooms, health facilities and government buildings, with tens of thousands of urban residents affected (Reuters, 2026).

The following sections of this chapter will examines how underlying social and economic conditions, patterns of settlement and land transformation, the configuration of critical systems and services, and the frameworks of flood risk governance interact to shape vulnerability, exposure, and coping capacity across the affected countries.

4.1 Sociodemographics

The flooding affected large areas in southern Mozambique and the northern part of South Africa. In 2022, the population in the province Limpo in northern South Africa was about 6.6 million (Parliament South Africa, 2025). The 2023 population in southern provinces of Mozambique was estimated to be 1.6 million (Inhambane), 1.5 million (Gaza), 2.5 million (Maputo) and around 1.1 millions for the city of Maputo (INE, 2024). Although the number has been declining over the last few decades, more than half of the population of Mozambique live in rural areas (World Bank, 2026). Vulnerability in rural and urban context differs, as described in more detail below. Some socioeconomic data at the country level for Mozambique, South Africa, Zimbabwe and Eswatini, including data on income and employment is provided in section 4.2.

Beyond the rural-urban divide, there are many demographic differences that affect vulnerability, including age, gender, migration background and socioeconomic status. As an example, in the South African province of Limpopo, Munyai et al. (2021) investigated the different factors present in relation to vulnerability in the Mopani district, these included (un)employment, education level, (dis)abilities, and household income.

During the January 2026 floods, more than 11,500 pregnant women and 164,049 women of reproductive age were estimated to be among the affected population, many residing in overcrowded shelters with reduced access to sexual and reproductive health services (Reliefweb, 2026). Pregnant women faced disproportionate risks related to increased nutritional and metabolic needs, vulnerability to dehydration and infection, and disruption of access to qualified obstetric and neonatal care. Stress and infectious exposure during floods are associated with adverse outcomes such as preterm birth and low birth weight (PubMed, 2024).

Children of 14 years or younger account for 44% of the total population in Mozambique, substantially higher than the global mean of 25% (World Bank, 2026). Young children are more vulnerable to flooding due to their physical limitations and dependence on caregivers. Therefore studies such as Mudavanhu et al. (2015), that highlight the lack of involvement of children in Disaster Risk Reduction in the Muzarabani District of Zimbabwe offer an opportunity for redress. Research has also shown that disasters can have sustained impact on the development of children far beyond the physical impact (see e.g. Peek, 2008 and Mort et al., 2018).

Lundgren & Strandh (2022) highlighted the social vulnerability to flooding in the southern Mozambique region, where recurring flooding events pushed the rural communities of the lower Limpopo River basin in a poverty spiral. For the city of Maputo with a population around 1.1 million inhabitants, around 50% of the population of Maputo was considered to be living below the poverty line (UN Habitat, 2010). Approximately 70% of the urban population of Mozambique lives in informal settlements (Spaliviero, 2006) and about 75% of the population of the South-African province of KwaZulu-Natal (Dlamini et al., 2024), south of Eswatini. These settlements, with poor housing conditions and infrastructure, are more vulnerable to flooding events (Zehra et al., 2019).

The Human Development Index (HDI) is a key metric that can indicate relative development, and includes data on life expectancy, education and per capita income. The HDIs for 2023 of the affected countries are (from high to low): 0.741 (South Africa), 0.695 (Eswatini), 0.598 (Zimbabwe) and 0.493 (Mozambique) as estimated by UNDP (2025). For a large part the South African HDI is also determined by regions outside the most affected area. Still, there remain strong regional differences with Estwatini and Zimbabwe considered part of the 'medium human development' group and Mozambique in the 'low human development' group. The low HDI in the region emphasizes its vulnerability to extreme weather events (Patt et al., 2010).

4.1.1 Health

The intersection of flood exposure and physiological vulnerability in Mozambique, South Africa, and Zimbabwe illustrates a clear case of compounding vulnerability and cascading risk. Flood hazards do not act in isolation; rather, they interact with pre-existing health conditions, social exclusion, and fragile infrastructure to amplify disaster impacts for specific population groups (Raju et al., 2022). Evidence from the region indicates that vulnerable groups, particularly the elderly, persons with disabilities, and those living with HIV, experience disproportionate impacts not because of exposure alone, but due to systemic barriers that undermine preparedness, response, and recovery capacities (Mangara et al., 2025; Masendeke, 2020).

Elderly individuals experience higher morbidity and mortality rates due to the convergence of pre-existing health conditions, reduced mobility, and limited access to timely evacuation and care (Bayraktar & Dal Yilmaz, 2018). The absence of age-responsive disaster planning, including assisted evacuation protocols and continuity-of-care mechanisms, means that delayed access to healthcare serves as a primary driver of post-disaster fatalities (Mangara et al., 2025). For persons with disabilities, flood risk is further intensified by inaccessible early warning systems and emergency shelters, which often lack ramps, adaptive sanitation, or appropriate support services. These structural exclusions force many to remain in high-risk locations, converting exposure into avoidable loss (Masendeke, 2020).

Physiological vulnerability is further compounded by immunological risk among people with chronic conditions such as HIV, tuberculosis (TB), and malnutrition. Southern Africa bears the highest burden of HIV globally, a context that significantly heightens disaster sensitivity (UNAIDS, 2023). Uninterrupted access to antiretroviral therapy (ART) and TB treatment is essential for survival; however, floods frequently disrupt these lifelines. Damage to healthcare facilities, loss of medical stocks, and destruction of cold-chain infrastructure impede treatment continuity, while flooded roads and transport systems prevent patients from reaching clinics (Kandawasvika et al., 2021; Naidoo et al., 2022). These disruptions trigger cascading health impacts, increasing risk of opportunistic infections, treatment failure, and HIV-related complications long after floodwaters recede.

Children represent another critical nexus of compounding vulnerability. Reports highlight that access to basic services such as healthcare, nutrition, and clean water is uncertain or unsafe in most flood-impacted areas, posing major health risks (UNICEF 2026). In Mozambique, where approximately 40% of children experience chronic malnutrition, flood-driven surges in waterborne pathogens such as *Vibrio cholerae* create acute, life-threatening conditions (UNICEF, 2026). These children are repeatedly exposed to floods and cyclones, with insufficient time or resources to recover nutritionally or physiologically between shocks, reflecting a pattern of erosive resilience rather than discrete disasters. With limited physiological reserves, malnourished children face mortality risks many times higher than their well-nourished peers during disease outbreaks (Save the Children, 2024).

Health vulnerabilities are further exacerbated during flood events by disruptions to critical infrastructure and services, increasing the likelihood of acute disease exacerbation and preventable mortality, particularly among individuals with chronic conditions (Muleia et al., 2024). In Mozambique, flood-induced disruption of food systems and health and nutrition services further deteriorated nutritional status in affected districts, increasing susceptibility to infectious diseases (Mugabe et al., 2021). The floods also occurred amid an active national cholera outbreak, with more than 1,700 reported cases and at least 26 deaths nationwide by early January 2026 (Beacon, 2026). Flooding magnified cholera transmission through contamination of water sources, population displacement, and overcrowded shelters, disproportionately affecting children, pregnant women, older adults, and malnourished individuals (Mugabe et al., 2021). As such, the cholera outbreak constitutes a major compounding factor, substantially increasing health risks during the flooding emergency (ACAPS, 2026).

4.2 Economic context, capacity, and livelihoods

Predominant livelihoods in the affected areas of Mozambique and Eswatini are various forms of agriculture and livestock keeping (CCARDESA, 2024, FEWSNET, 2014), while areas in South Africa, such as Limpopo, and Masvingo province in Zimbabwe, also rely on formal and informal mining (FEWSNET, 2011, Limpopo Provincial Government, 2025). Tourism is another key industry, especially in Limpopo linked to Kruger National Park, which has been closed due to floods and previous floods caused substantial economic damage (Abrams et al., 2021, BBC, 2026, Dube et al., 2023).

Agriculture dominates local livelihoods and contributes significantly to national GDP and employment, especially in Mozambique and Zimbabwe (see table 4.1 for details). Moreover, poverty is high: 65% of Mozambicans, 58.9% in Eswatini, and 38.4% in Zimbabwe live below the national poverty line (see table 4.1 for details). Climate-induced hazards thus threaten livelihoods, national economic performance, and food security. First analysis show 54% of flooded areas in Mozambique are agricultural land (Copernicus EMS, 2026), with over 10,000 hectares lost in Buzi district, Sofala province, and more than 27,000 livestock affected (OCHA, 2026, OCHA, 2025, IOM, 2026). South Africa also reported severe damages of farm buildings and storerooms (Government South Africa, 2026).

Table 4.1: *Basic economic and livelihood indicators for most recent values compiled from open access data from World Bank, accessed 22.01.26. *Inflation rate data retrieved from IMF accessed 22.01.26*

Indicator	Mozambique	South Africa	Eswatini	Zimbabwe
GDP per Capita (PPP, current international $) in 2024	1.705$ (2024)	15.456$ (2024)	11.799$ (2024)	5.928 $ (2024)
Poverty headcount ratio at national poverty lines (% of population)	65% (2022)	NA	58,9% (2016)	38,39% (2019)
Inflation rate (average consumer prices, annual in %)*	4,9% (2025)	3,4% (2025)	3,5% (2025)	89% (2025)
Agriculture, forestry, and fishing, value added (% of GDP)	25,18% (2024)	2,81% (2024)	6,48% (2024)	8,69% (2024)
Employment in agriculture (% of total employment) (modeled ILO estimate)	69,58% (2023)	18,79% (2023)	13,77% (2023)	52,53% (2023)

Employment in industry (% of total employment) (modeled ILO estimate)	9,06% (2023)	17,69% (2023)	18,47% (2023)	12,35% (2023)
Unemployment, total (% of total labor force) (national estimate)	6,06% (2022)	32,28 % (2024)	34,61% (2023)	9,29% (2023)

Food security is already stressed or in crisis in large parts of affected areas of Mozambique and Eswatini (IPC, 2025, WFP, 2024). Before the floods, projections in October 2025 estimated 2.67 million people would face high acute food insecurity (IPC 3+), with 170,000 in Emergency (IPC Phase 4), primarily due to prolonged droughts since 2023 (IFRC, 2025, FAO, 2024). Zimbabwe has not reported widespread food insecurity, but the floods and prior inflation over 700% in 2024 and around 90% in 2025 will likely affect livelihoods, food security, and health expenditures post-floods (IMF, 2025).

Recurrent flooding, alongside cyclones and droughts, can progressively erode community coping capacity, increasing losses and vulnerabilities. In Mozambique, persistent socio-economic vulnerability combined with recurring hazards contributes to cycles of poverty and food insecurity, limiting savings and long-term resilience (Lundgren & Strandh, 2022). However, post-Cyclone Idai analyses show that after short-term shocks, communities have diversified livelihoods, relying less on agriculture and more on small businesses and formal wage employment (IV & Yu, 2025). This may be due to effective recovery initiatives, but other initiatives such as resettlement have threatened livelihood sustenance, increasing people's vulnerability (Jacobs & Almeida, 2020; Goswami et al, 2026).

In Zimbabwe's Matabeleland, farmers face drought, low purchasing power, an inability to hire labor, and frequent poor harvests due to repeated hazards (Nyathi, 2024). Moreover equipment is often destroyed as seen during Idai (Munsaka et al., 2021). These problems are compounded by land-tenure insecurity, as post-2000 resettlement initiatives for dispossessed households during colonial occupation failed to declare legal land ownership. Farmers are facing evictions, discouraging investment in irrigation and other productivity-enhancing assets (Nyathi, 2024). Similarly, historical inequalities in the Limpopo basin have distanced smallholder farmers from policy processes and hampered equitable access to natural resources, including land and water (GWP, 2014).

Flood impacts are not confined to rural areas. Colonial-era spatial planning, a dynamic political environment, governance challenges, and insufficient infrastructure are critical factors increasing Southern Africa's flood vulnerability, with marginalized communities often located in floodplains and lack resources for resilience (Amnesty, 2025; Byaruhanga, 2025). In urban centers, floods destroy homes and disrupt livelihoods, causing job loss and displacement, as seen in KwaZulu-Natal and Gauteng in South Africa and in Bulawayo and Masvingo, Zimbabwe (Raphela, 2025; Hlahla et al., 2022; Sverdlik et al., 2024). Further, vulnerability, exposure and impacts are often gendered: in KwaZulu-Natal, 68.1% live in poverty, with women forming the majority of the low income groups and those living in low-income households (Statistics South Africa, 2017). For instance, in Pietermaritzburg women often care for 4–6 dependents while relying on informal work or aid -

making them susceptible to flood impacts, income loss, water insecurity, and food insecurity, a pattern also seen in Bulawayo (Raphela, 2025; Hlahla et al., 2022).

In Mozambique, livelihoods exhibit additional complexities. Declining livelihoods and economic pull factors in urban areas coincide with high population movements from conflict and hazard displacement. There are an estimated 461,000 Internally Displaced Persons (IDPs) in Northern Mozambique and a further 148,000 IDPs in Central Mozambique (UNHCR, 2025). Beira, the capital of Sofala Province, hosts a significant number of climate-related IDPs, which in turn remain at risk of further cyclones and flooding (IOM,2025). Beira itself was previously devastated by Cyclone Idai, illustrating the precarity that many people already displaced by weather-related disasters or conflict face.

IDPs often face extreme poverty, rely on informal economies, and may experience conflict with host populations over limited livelihood resources (CGIAR, 2024). Displacement has furthermore increased early marriages and transactional sex as coping strategies for women and girls, particularly orphans (CGIAR, 2024). For instance, transactional sex as a coping strategy has also been reported in exchange for water access in Bulawayo, Zimbabwe (Nyathi, Ndlovu & Mpahosa, 2025).

4.3 Spatial planning and exposure

Flooding has had particularly severe consequences for cities and towns in Mozambique and South Africa, where dense populations, unregulated housing, and compromised basic services have translated rainfall into large-scale displacement and infrastructure disruption (UN News, 2026). In both countries, rapid urbanisation without adequate planning has expanded informal settlements into flood-prone zones with poor drainage and limited basic services (Dua, Z., 2019). Gaps in early warning dissemination—messages not reaching informal settlements, not being trusted, or not being actionable for people without safe places to go—mean that many households cannot evacuate in time even when hazards are forecast (Anticipation Hub, 2024).

In Mozambique, extensive use of non-engineered adobe housing - generally built with sun-dried earth and straw that are structurally weakened after a few days of rain- is estimated at around 90% of homes, which can mean that prolonged rainfall rapidly translates into structural collapse and large-scale displacement (Antonio, 2018; UN OCHA, 2026).

Both Mozambique and the affected provinces of South Africa have substantial populations living below or near the poverty line, with limited savings, low insurance coverage, and high dependence on climate-sensitive livelihoods, all of which increase vulnerability to flooding (Climate Risk Index, 2026). Urban impacts are especially pronounced in Gaza’s capital Xai-Xai and in towns across the South African provinces of Limpopo and Mpumalanga (WMO, 2026). The floods disproportionately affect communities settled on low-lying riverbanks, floodplains and informal peri-urban areas, including people living in high-density settlements along the Limpopo, Incomati, and other basins. In both countries, rapid urbanisation without adequate planning has expanded informal settlements into flood-prone zones with poor drainage and limited basic services (Li, 2025). High population density in affected corridors, combined with limited access to safe evacuation options and social protection, increases exposure and reduces the capacity to relocate safely (UN News, 2026).

4.4 Land-use and land cover change

The biophysical conditions of the Limpopo basin in Mozambique mean that agriculture is very susceptible to drought and flooding making the people who rely on agriculture vulnerable and food insecure (LIMCOM, 2026). In Mozambique the flooding has submerged more than 70,000 hectares (173,000 acres) of crops, deepening food shortages for small-scale farmers in a country already struggling with poverty, cyclones and other natural hazards (Al Jezeera, 2026).

This combination of chronic drought interspersed with flooding increases the risk and vulnerability to farmers, who hesitate to invest in new technologies, despite existing infrastructure for smallholder irrigation being largely dysfunctional (GWP, 2014). The increase in population density in recent years has also led to intensive exploitation of natural resources, resulting in a high level of land degradation (FAO, 2004). While one sixth of the basin is covered by wetland - which can reduce the impact of floods - these areas are under strain as agricultural activity and human settlements increase (CGIAR, 2006).

Land use in the upper Mzingwane River basin (the portion of Zimbabwe located in the Limpopo River basin) consists mostly of commercial farming while communal land and subsistence agriculture are practiced in the lower basin. The communal lands are considered to be vulnerable because they are dry, have poor soils, and are not suitable to rainfed agriculture. The agricultural sector has been significantly impacted, with flooding and hailstorms damaging crops at various growth stages, including maize, horticulture, and small grains. Waterlogging has reduced crop yields in some areas, while hailstorms have destroyed standing crops, threatening household food security and income sources (IFRC, 2026).

4.5 Critical systems and services

The intense, consecutive rainfall events during this period exposed significant weaknesses in existing infrastructure, the majority being designed for less intense, historical weather patterns (CSVR, 2026; Libera, 2026). Such damage to critical systems significantly impacts vulnerable populations. For instance, health vulnerabilities are further exacerbated by disruptions to critical infrastructure and services during flood events.

In central and southern Mozambique, floods and cyclones have damaged transport networks and health facilities, severely constraining access to essential services during emergencies.UN reports indicate nearly 5,000 km of roads were damaged, including sections of the main highway connecting Maputo to the rest of the country, significantly hindering the transport of goods, delaying emergency referrals, and disrupting pharmaceutical supply chains (OCHA, 2026). These breaks in supply and service increase the likelihood of preventable mortality, particularly among individuals with chronic conditions (Muleia et al., 2024). Similarly, in Zimbabwe access and mobility have been affected as bridges, roads and infrastructure have been significantly damaged or destroyed (Al Jezeera,2026; NAP, 2024).

In many municipalities in South Africa, for instance, drainage infrastructure has not kept pace with the rate of urbanisation. Decades of lack of sufficient investment, maintenance or improvements to the infrastructure have further compromised the systems (Kunene et al., 2021). Studies from South

Africa highlight that many urban areas lack effective stormwater systems, while residents report recurrent flood damage to vegetation, soil stability and housing, often without sufficient financial assistance from municipalities (Byaruhanga, 2025). For example, in KwaZulu-Natal the destruction of natural buffers due to development and agriculture has also increased the risk of floods (NSRI, 2024).

The flood resilience of cities is intricately linked to governance structures, policies, and practices that shape their ability to respond to challenges and promote sustainable development. As such addressing Southern Africa's flood risk requires a phased and multi-level strategy. Suggestions include setting up inclusive early warning systems and upgrading drainage infrastructure in flood-prone urban areas and informal settlements (World Bank Group, 2012). In the medium term, investment in nature-based solutions such as wetland restoration, riparian buffers, and green infrastructure prioritize enhanced water absorption and flood regulation. In the long term, sustained investment in research and innovation is necessary to refine localized flood risk assessments, improve data in under-served areas, and test ecosystem-based adaptation strategies (Byaruhanga, 2025; SA Cities Network, 2022).

4.6 Flood risk management

4.6.1 Governance

Mozambique, South Africa, Eswatini, and Zimbabwe are connected through transboundary river systems. Flood risk governance in these countries is led by national disaster management and water-sector institutions, with varying mandates covering disaster risk reduction, early warning, response coordination, and regional cooperation. The Limpopo Watercourse Commission (LIMCOM) and the Zambezi Watercourse Commission (ZAMCOM) facilitate cooperation, data sharing, and joint planning for these shared river systems. These include opportunities for Transboundary water management (GCA, 2022).

In Mozambique, flood and cyclone risk management is coordinated by the National Institute of Disaster Management (INGC), which operates under the Ministry of State Administration (UNDRR, 2024). INGC is mandated to lead national emergency preparedness and response, promote disaster risk reduction, and ensure cross-sectoral coordination across government (INGC, 2026). A core function of the institute is the coordination of early warning systems for floods and cyclones, including the dissemination of alerts and the alignment of response actions across sectors. Given Mozambique's downstream position in several major river basins, INGC plays a critical role in managing flood impacts that originate upstream and in engaging with regional partners on preparedness and response (Hellmuth et al., 2007).

In South Africa, flood risk management is led by the Department of Water and Sanitation (DWS), which is responsible for overseeing flood risk assessments, hydrological monitoring, and the resilience of water-related infrastructure. DWS works closely with the Water Research Commission and the South African National Space Agency to develop flood modelling, forecasting, and decision-support tools, including the use of satellite-based data. Through these technical and scientific functions, South Africa contributes significantly to the generation of upstream hydrological information that is relevant for flood preparedness and early warning in downstream countries sharing the same river basins (Department of Water and Sanitation, n.d.; SANSA, n.d.).

In Eswatini, responsibility for flood-related disaster risk management lies with the National Disaster Management Agency (NDMA). The agency is mandated to coordinate disaster risk management activities, including floods, with a strong focus on capacity building, preparedness, and early warning systems. NDMA leads the coordination of response efforts across government and supports community-level readiness, particularly in areas exposed to riverine flooding. Its role is especially important in managing flood risks linked to transboundary rivers shared with South Africa and Mozambique (GFDRR, 2020).

In Zimbabwe, flood risk management and disaster response are coordinated by the Civil Protection Department under the Ministry of Local Government and Public Works. The department is responsible for national preparedness, response coordination, and recovery related to flood events, and it represents Zimbabwe in transboundary river basin institutions. However, assessments of Zimbabwe's flood preparedness indicate that disaster governance remains largely reactive, with limited financial and material resources constraining effective preparedness and risk reduction. Strengthening legislative frameworks for disaster risk reduction presents an opportunity to shift flood management from a reactive response towards more effective preventative and risk-informed approaches (Mavhura, 2020).

4.6.2 Policies and plans

Building on the institutional governance mechanisms described above, all four countries have established policies and plans that address flood risk management, although the extent to which these frameworks translate into effective flood protection mechanisms varies across the region. The Southern African Development Community (SADC) has championed the advancement of regional integration yet there is still a lack of policy coherence and need to address knowledge gaps and improve sectoral integration at both regional and national levels (Kalonga, et al, 2025). A further longer term challenge are the technical, financial and political constraints including a perceived lack of coordination amongst actors (Lourenço Neves, 2024).

In Mozambique, flood risk governance is guided by a comprehensive policy and legislative framework that places strong emphasis on prevention and preparedness. The National Disaster Management Policy and the Disaster Management Law establish a clear mandate for disaster risk reduction, preparedness, response, and recovery, coordinated through the National Institute for Disaster Management (INGC) (Government of Mozambique, 2024). These principles are operationalised through the Master Plan for Disaster Risk Reduction 2017–2030, which seeks to strengthen early warning systems, reduce vulnerability, and improve institutional coordination.

In South Africa, flood risk management is underpinned by a combination of water, disaster management, and climate adaptation policies. The National Water Act (1998) and the National Disaster Management Act (2002) provide the legal foundation for managing flood risks with the Department of Water and Sanitation implementing the National Flood Studies Programme (DWS, n.d.). These are complemented by the Climate Change Adaptation Response Plan (2025), which is focused on coastal flooding as a growing risk with significant social and economic costs. Despite this relatively strong policy framework, recent flood events have highlighted persistent implementation gaps. High recovery costs place strain on household resources, while rapid urbanisation and inadequate spatial planning have increased exposure to flood hazards. In addition, weaknesses remain in the dissemination of early warnings and in evacuation planning that is sufficiently tailored to community needs, limiting the effectiveness of existing flood protection measures (Amnesty, 2025; Libera, 2026).

In Eswatini, flood risk management is guided by the Disaster Management Act (2006) and the National Disaster Management Policy, which define the mandate of the National Disaster Management Agency. These frameworks emphasise preparedness, early warning systems, and coordinated response, particularly for flood risks associated with shared river basins. While these policies provide a basis for coordinated flood risk management, implementation remains focused on non-structural measures, with limited evidence of extensive flood protection infrastructure across flood-prone areas (GFDRR, 2020).

In Zimbabwe, flood risk management is anchored in the Civil Protection Act (1989) and supported by the National Climate Policy. The Civil Protection Department implements these frameworks through instruments such as the National Contingency Plan and through engagement in transboundary river basin institutions. However, despite the presence of policy frameworks, flood protection mechanisms are constrained by limited financial and material resources. As a result, implementation has focused more on emergency response and coordination than on preventative or structural flood protection measures (CRIDF, 2021).

4.6.3 Early warning and early action

While all four countries have made progress toward multi-hazard early warning systems, the maturity, coverage, and integration of anticipatory action vary, with significant potential for strengthened regional coordination. They are all part of the broader SADC regional effort, formalized by the Maputo Declaration (2022), which commits member states to enhancing early warning and early action (UNDRR, 2022). All four countries are also included in the regional Early Warnings for All (EW4All) initiative (WMO, n.d.), with Mozambique and South Africa having developed national roadmaps.

In Mozambique, early warning for floods is embedded within a national Multi-Hazard Early Warning System (MHEWS), supported by the Disaster Risk Management Act (2020), which provides the legal basis for early warning and early action (UNDRR, 2024). The National Institute of Meteorology (INAM) is responsible for the production and dissemination of weather forecasts and warnings, while the National Directorate of Hydraulic Resources Management (DNGRH), under the Ministry of Public Works, Housing and Water Resources, plays a complementary role in water resources management and in the prevention and mitigation of flood impacts (UNDRR, 2024).

Mozambique has developed an Early Action Protocol (EAP) for floods covering the Limpopo, Buzi, Zambezi, and Licungo river basins, which was activated during the December 2025 flood event (IFRC, 2025). Evidence from recent assessments of people's experiences of anticipatory action highlights both the life-saving potential of these mechanisms and the importance of improving last-mile dissemination and community understanding (WFP, 2025).

In South Africa, flood early warning is anchored in a technically advanced forecasting environment (IMESA, 2024). The South African Flash Flood Guidance (SAFFG) system forms a core component of the national Flood Early Warning System and is managed primarily by the South African Weather Service. The country's upstream position in several shared river basins gives it significant potential to support transboundary early warning through the provision of hydrometeorological data and forecasts to downstream neighbours.

In Eswatini, flood early warning forms part of a developing Multi-Hazard Early Warning System led jointly by the Eswatini National Meteorological Services and the National Disaster Management Agency. Current efforts focus on strengthening forecasting, early warning dissemination, and preparedness, particularly for flood risks associated with the Limpopo River Basin. Although still evolving, Eswatini's early warning system is increasingly aligned with regional approaches and benefits from transboundary cooperation mechanisms that support shared monitoring and preparedness (UNDP, n.d.; UNDRR, 2024).

In Zimbabwe, flood early warning relies on coordination between the Meteorological Services Department, the Civil Protection Department, and community-level warning and response mechanisms (GFDRR, 2018; World Bank, 2022). This is complemented by anticipatory action protocols for floods developed with support from the Food and Agriculture Organization, which aim to trigger early actions ahead of forecasted flood impacts (Anticipation Hub, n.d.; FAO, 2023). While these systems strengthen preparedness at national level, their effectiveness is influenced by resource limitations and by the need for more systematic integration of scientific forecasts with community-based dissemination and response (WFP, 2025).

The transboundary nature of the affected river basins underscores the need for stronger regional integration. Strengthening basin-level cooperation has the potential to improve the timeliness and effectiveness of early warnings and anticipatory actions, reducing flood impacts across national borders and strengthening collective resilience in Southern Africa.

4.6.4 Emergency response

In Mozambique, the scale and severity of flooding prompted the government to declare a national emergency and activate its full disaster management system. An Emergency Operations Centre was established to coordinate response efforts, particularly in the heavily affected provinces of Gaza, Maputo, and Sofala (United Nations Office at Geneva, 2026). Nationwide red alerts were issued to mobilise assistance and support large-scale evacuations from high-risk areas. Search-and-rescue teams were deployed, and tens of thousands of people were relocated to temporary shelters as flooding caused widespread infrastructure damage and disrupted supply routes. Evacuations remain ongoing in areas such as Xai-Xai, where floodwaters continue to pose serious risks. Recognising the magnitude of the crisis, the government formally appealed for international assistance, including United Nations support for logistics, rescue operations, and the delivery of humanitarian aid (United Nations Office at Geneva, 2026; Africa News, 2026).

In South Africa, a national disaster declaration was issued to enable coordinated relief efforts and the mobilisation of resources across the worst-affected provinces, including Limpopo, Mpumalanga, KwaZulu-Natal, the Eastern Cape, and North West (South African Red Cross, 2026). In parallel, Limpopo Province declared a provincial state of disaster in response to extensive flooding (Mashamaite, 2026). Emergency response has included the deployment of the South African National

Defence Force alongside emergency services, using helicopters and boats to evacuate residents, rescue stranded individuals, and deliver essential supplies to isolated communities. Authorities have also implemented area closures, such as in Kruger National Park, to reduce risk to the public, while repair works on critical infrastructure are underway and search-and-rescue operations continue (South African Red Cross, 2026; Mosqueda, 2026).

In Eswatini, no formal national emergency declaration has been reported, reflecting a comparatively more localised impact of flooding. The government, working through the National Disaster Management Agency, has focused on rapid assessments and the provision of food aid and basic assistance to affected households. Response efforts have been supported by humanitarian partners, with the Red Cross noting the timeliness of the government's actions. Public advisories have been widely disseminated, urging communities to avoid flooded areas and other high-risk locations, emphasising risk awareness and safety rather than large-scale evacuation or military deployment (Swazi Daily News, 2026).

In Zimbabwe, while no formal national emergency declaration has been announced, the government has taken early response measures by releasing emergency funds to districts to support preparedness and response ahead of continued heavy rainfall. Local authorities and disaster management teams have been actively engaged in raising public awareness, coordinating rescue and relief efforts, and distributing assistance where access allows. These actions indicate a decentralised response approach, with emphasis on preparedness and local-level coordination in anticipation of further flooding (IFRC GO, 2026).

4.6.5 Individual and household coping behaviors

Information on the individual and household coping behaviors are often anecdotal in nature and available from various news reports. Overall, a pattern emerges that across the affected region, people have attempted to reach higher ground to escape from the danger. News outlets report on people fleeing to (public) buildings or high-lying areas in the region, and about people climbing the roofs of their homes. The decision to flee to a higher floor or rooftop of a building (vertical) versus towards a safer area in the region (horizontal) is a decision that can have a large impact on chance of survival, but in many cases a rushed decision has to be made (based on insights from past flooding events in Japan; Mizumura et al., 2025 and Mizumura & Nakamura, 2025).

Below are some reports provided from the individual countries in the affected regions:

- For the Gaza province in Mozambique, reports indicate that many people have fled their homes to find shelter in schools or churches (AP News, 2026). Some stranded residents in Mozambique climbed their roofs as a last resort (Reuters, 2026).
- In South Africa, around 600 visitors and staff of the Kruger National Park have fled to high-lying regions in the park and were evacuated from there (AP News, 2026).
- Authorities in Zimbabwe have stated that citizens should better follow the issued warnings and state that recent casualties could have been prevented if warnings are taken more seriously (ZBC News, 2026).
- In the Pine Valley area of Eswatini, an improvised bridge was created by felling a large tree (Times of Eswatini, 2026).

4.6.6 Insurance and social protection

In Mozambique, the primary mechanism for shock-responsive social protection (SRSP) is the Direct Social Support Programme - Post-Emergency (PASD-PE), managed by the National Institute of Social Action (INAS). PASD-PE was adapted after Cyclone Idai in 2019 to respond to rapid-onset shocks, including using existing social protection caseloads, sharing beneficiary data between INGD and INAS, and improving registration and digital payment tools (IPC-IG & WFP Mozambique, 2022).

Since the floods began, supply chains have been significantly disrupted, with authorities reporting losses of more than 27,000 heads of livestock (UNOCHA, 2026). As in previous shocks, these disruptions are likely to drive food price volatility and increased insurance claims. Insurers face higher claims from infrastructure damage and crop losses, which can translate into tighter coverage terms and higher premiums over time (ASA, 2026). Evidence indicates that insurance coverage for flood losses remains very low, especially for poorer households and informal settlements, due to high premiums and the informal nature of housing (UNDP, 2024). While household-level flood insurance remains largely inaccessible, insurance plays a vital role at the macro-institutional level. Mozambique has leveraged sovereign parametric insurance through the African Risk Capacity (ARC) and the World Bank's Catastrophe Deferred Drawdown (Cat DDO). These mechanisms provide the government with rapid liquidity once pre-defined rainfall or river-gauge thresholds are met, which in turn funds the PASD-PE scale-up and infrastructure repair (ARC, 2025; IPC-IG & WFP Mozambique, 2022).

South Africa has social protection instruments that have been flexibly used in crisis periods (e.g., COVID-19), but there is limited evidence of a purpose-built SRSP scheme being systematically scaled up specifically for floods to the same degree as in other low-income countries. Flood insurance plays an important role for better-off households and businesses through private non-life insurance. After the 2022 KwaZulu-Natal floods, non-life insurers and banks rapidly mobilised to process a very large volume of homeowner, household-contents, motor, and commercial claims, waving excesses in some cases and describing hundreds of millions of rand in insured losses (SAIA, 2022). But penetration is highly unequal, and flood insurance is not a central pillar of recovery for the poorer in the most affected communities, who rely far more on government and humanitarian assistance, family networks, and people's own savings (Lefutso et al., 2024).

Zimbabwe's main national social assistance schemes include the Harmonised Social Cash Transfer (HSCT) for labour-constrained, food-poor households and a Public Assistance programme, both under the Ministry of Public Service, Labour and Social Welfare. There is a clear policy push to make these SRSP more shock-responsive, but large-scale vertical or horizontal scale-ups of national social protection during flood events remain limited (Cash Hub, 2021). At the macro level, Zimbabwe participates in ARC sovereign parametric insurance and a 2020 ARC payout of about USD 1.4 million to the Government of Zimbabwe (plus additional Replica funds to WFP) supported drought response (ARC, 2020). But insurance is not a major factor in household-level recovery from floods, given very low penetration of individual flood or property insurance and high poverty (World Bank, 2012).

Eswatini has core social assistance programmes and an explicit policy agenda to make them more shock-responsive (World Bank, 2021), but there is limited evidence of large, systematic flood-specific scale-ups comparable to some neighbouring countries. Flood insurance is not currently a significant factor in recovery for most flood-affected households in Eswatini. Recovery is driven instead by government social assistance, school feeding, neighborhood care points, and humanitarian relief and cash/food assistance (Cash Hub, 2021).

5 Summary of findings

Exposure in the region is very high due to aging infrastructure, the degradation of ecosystems that previously provided natural flood defences, and the widespread use of housing materials that is very susceptible to flood damage. Vulnerability is also high, driven by food insecurity, cascading risks arising from multiple interacting hazards, and entrenched cycles of poverty. Climate variability associated with ENSO is an important driver of extreme rainfall in the region, with observations indicating that the La Niña conditions this rainy season have increased rainfall intensity by around 22%, approximately half the size of the increase that is observed with long-term global warming.

While climate models have known limitations in representing extreme rainfall processes in the region, the broader literature documents increasing trends in extreme precipitation across different subregions, rainfall durations, and seasons suggests that confidence is now higher than in AR6 that climate change is influencing such events. However, the range of extreme rainfall driving mechanisms in the region, the uniqueness of the current event, and challenges around model capabilities mean that further study is required, using both probabilistic and other attribution approaches, to quantify how much of the observed changes are due to climate change.

All drivers of risk: exposure, vulnerability and the hazard itself have increased in recent years, contributing to the devastating impacts of the heavy rainfall, thus both adaptation and mitigation are essential to reduce risks. Adaptation that focuses on reducing vulnerability, as well as improving infrastructure and restoring ecosystems and mitigation centred on a just transition away from fossil fuels.

Data availability

All time series used in the attribution analysis are available via the Climate Explorer.

References

All references are given as hyperlinks in the text.

Appendices

A1 Data and methods

A1.1 Observational data

We first use observational and reanalysis data to estimate the return period of a similar event in the present day and to assess the historical trends with increasing GMST and ENSO. The datasets used are as follows:

ERA5 - The European Centre for Medium-Range Weather Forecasts's 5th generation reanalysis product, ERA5, is a gridded dataset that combines historical observations into global estimates using advanced modelling and data assimilation systems (Hersbach et al., 2020). We use daily precipitation data from this product at a resolution of 0.25°×0.25°. We use reanalysis data until the end of December, extended with analysis data for January to cover the period of the event. Data used in the main analysis was obtained from KNMI's Climate Explorer tool. We extend the re-analysis data with the ECMWF analysis (1-18 January) and the ECMWF forecast (19 July) to cover the period of the event.

CPC - This is the gridded product from NOAA PSL, Boulder, Colorado, USA, known as the CPC Global Unified Daily Gridded data, available at 0.5° x 0.5° resolution, for the period 1979-present. We use daily precipitation data.

MSWEP - The Multi-Source Weighted-Ensemble Precipitation v2.8 dataset (updated from Beck et al., 2019) is fully global, available at 3-hourly intervals and at 0.1° spatial resolution, available from 1979 to ~3 hours from real-time. This product combines gauge-, satellite-, and reanalysis-based data, including ERA5.

TAMSAT - The Tropical Applications of Meteorology using SATellite and ground based observations, Maidment et al., (2017), is a daily rainfall dataset based on using high-resolution thermal-infrared observations to identify precipitating clouds. Daily rainfall data are available at 0.0375° x 0.0375° spatial resolution over the African continent from 1983 to the present.

CHIRPS - The rainfall product developed by the UC Santa Barbara Climate Hazards Group called "Climate Hazards Group InfraRed Precipitation with Station data" (CHIRPS; Funk et al. 2015). Daily data are available at 0.05° resolution, from 1981-31 December 2025. The product incorporates satellite imagery with in-situ station data.

As a measure of anthropogenic climate change we use the (low-pass filtered) global mean surface temperature (GMST), where GMST is taken from the National Aeronautics and Space Administration (NASA) Goddard Institute for Space Science (GISS) surface temperature analysis (GISTEMP, Hansen et al., 2010 and Lenssen et al. 2019).

As a measure of the El Niño - Southern Oscillation cycle (ENSO) we use the detrended Niño3.4 index. This is computed from NOAA's ERSST v.5 sea surface temperatures, by subtracting the mean tropical SST (20S-20N) from the mean SST over the Niño3.4 region (5S-5N, 170W-120W). This index is therefore adjusted to remove the linear trend associated with climate change as proposed in van Oldenborgh et al., 2021, but without rescaling each calendar month.

A1.2 Model and experiment descriptions

We use 2 ensembles of climate models from climate modelling experiments using very different framings (Philip et al., 2020): Sea Surface Temperature (SST) driven global circulation high resolution models, coupled global circulation models and regional climate models.

1. **CORDEX**

Coordinated Regional Climate Downscaling Experiment CORDEX-CORE over the Africa domain with 0.22 km resolution (AFR-22;Giorgi and Gutowski, 2015; Giorgi et al., 2021) and with 0.44 km resolution (AFR-44; Nikulin et al., 2012). The ensemble used consists of AFR-22 and AFR-44 together with different combinations of 7 regional climate models and downscaling 11 GCMS, resulting in 37 combinations. These simulations are composed of historical simulations up to 2005, and extended to the year 2100 using the RCP8.5 scenario.

2. **HighResMIP**

The High Resolution Model Intercomparison Project — SST-forced model ensemble (Haarsma et al. 2016), the simulations for which span from 1950 to 2050. The SST and sea ice forcings for the period 1950-2014 are obtained from the 0.25° x 0.25° Hadley Centre Global Sea Ice and Sea Surface Temperature dataset that have undergone area-weighted regridding to match the climate model resolution. For the 'future' time period (2015-2050), SST/sea-ice data are derived from RCP8.5 (CMIP5) data, and combined with greenhouse gas forcings from SSP5-8.5 (CMIP6) simulations (see Section 3.3 of Haarsma et al. 2016 for further details).

A1.3 Statistical methods

Methods for observational and model analysis and for model evaluation and synthesis are used according to the World Weather Attribution Protocol, described in Philip et al., (2020), with supporting details found in van Oldenborgh et al., (2021), Ciavarella et al., (2021), Otto et al., (2024) and here. The key steps, presented in sections 3-6, are: (3) trend estimation from observations; (4) model validation; (5) multi-method multi-model attribution; and (6) synthesis of the attribution statement.

In this report we analyse the time series of DJF seasonal maxima of 10-day accumulated rainfall (DJF Rx10day), area-averaged over the study region described in Section 1.2. A nonstationary Generalised Extreme Value (GEV) distribution is used to model DJF Rx10day. For rainfall, the distribution is assumed to scale exponentially with the covariates, with the dispersion (the ratio between the standard deviation and the mean) remaining constant over time, to account for the dependence of maximum moisture content that the atmosphere can hold in accordance with the Clausius-Clayperon relationship (Trenberth et.al., 2003, O'Gorman and Schneider 2009). The parameters of the statistical model are estimated using maximum likelihood.

For each time series we calculate the return period and intensity of the event under study for the 2026 GMST and for 1.3°C cooler GMST: this allows us to compare the climate of now and of the preindustrial past (1850-1900, based on the Global Warming Index), by calculating the probability ratio (PR; the factor-change in the event's probability) and change in intensity of the event.

In order to examine the effect of the ENSO phase on DJF Rx10day alongside that of increasing GMST, we extend the nonstationary model to accommodate an additional covariate. In this case, the variable of interest, $DJF\ Rx10day$, is assumed to follow a GEV distribution in which the location and scale parameters vary with both GMST and ENSO:

$$X \sim GEV(\mu, \sigma, \xi \mid \mu_0, \sigma_0, \alpha, \beta, T, I),$$

where X denotes the variable of interest, rainy-season precipitation; T is the smoothed GMST; I is the detrended Niño3.4 index for the OND season; μ_0, σ_0 and ξ are the location, scale and shape parameters of the nonstationary distribution; and α, β are the trends due to GMST and ENSO, respectively. As a result, the location and scale of the distribution have a different value in each year, determined by both the GMST and Niño3.4 states. Maximum likelihood estimation is used to estimate the model parameters, with

$$\mu = \mu_0 exp\left(\frac{\alpha T + \beta I}{\mu_o}\right) \quad \text{and} \quad \sigma = \sigma_0 exp\left(\frac{\alpha T + \beta I}{\mu_o}\right).$$

This formulation again reflects the Clausius-Clapeyron relation, which implies that precipitation scales exponentially with temperature, and so that precipitation will scale exponentially with the strength of the detrended Niño3.4 index. Under this model, the effects of GMST and the detrended Niño3.4 index are assumed to be independent of one another, so that the change in intensity due to GMST is unaffected by the change in intensity due to the ENSO phase. We note that this may not be the case in the real world, as the intensity and frequency of El Niño events may have been influenced by climate change (Cai et al., 2021); however, by using a detrended Niño3.4 index (see Section 2.1) we aim to minimise the correlation between the two factors, and so do not expect the qualitative findings of this study to be affected by this simplifying assumption.

The results summarising the contributions from GMST and Niño are quoted in the main report, for both cases- (1) DJF Rx10day ~gmst and (2) DJF Rx10day ~gmst+NiñoOND. As explained in Section 2, all of the observed datasets reflect the dependence of extreme rainfall in the region to both GMST and ENSO, with considerable contributions from both phenomena. However, due to the climate models considered for this study being unable to simulate the relationship between extreme rainfall and ENSO in the region, we limit the ENSO analysis to observations alone.

A1.3.3 Defining the ENSO state in climate models

The multi-method multi-model attribution step of the WWA protocol involves estimating, for each climate model, the effective return level of a 1-in-*n*-year event under the current climate state, and estimating the expected change in likelihood and intensity of such an event after a specified change in the covariates. Because the smoothed GMST is generally monotonically increasing, the standard WWA approach is simply to take the model's 2024 GMST as a covariate and to estimate the expected magnitude of an *n*-year event. However, the factual climate in this study is defined by the 2024 GMST and by the mean of the detrended Niño3.4 index during the rainy season. During the attribution step, the detrended Niño3.4 index derived from the climate model is standardised so that the subset from 1979-2024 has mean 0 and variance 1; the 'factual' climate is then defined as having the model's 2024 GMST and the 2024 observed value of the detrended Niño3.4 index, standardised in the same way. This removes any potential biases in the results due to differences between the amplitude of the modelled Niño3.4 index and that observed.

A2 Model evaluation figures

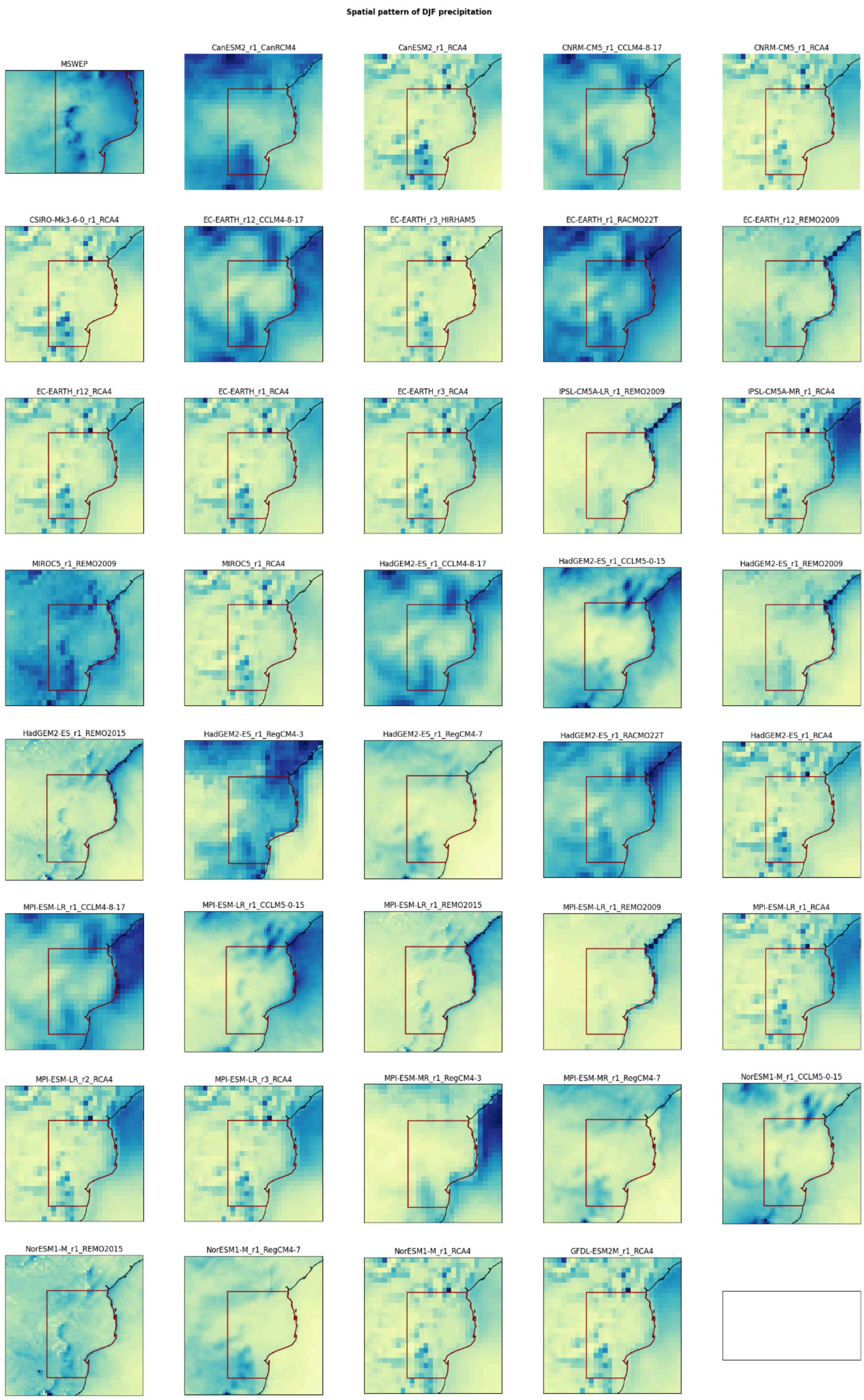

Figure A.2.1: *Spatial patterns of DJF precipitation in observations and CORDEX models. The study region for the rainfall analysis is highlighted in red.*

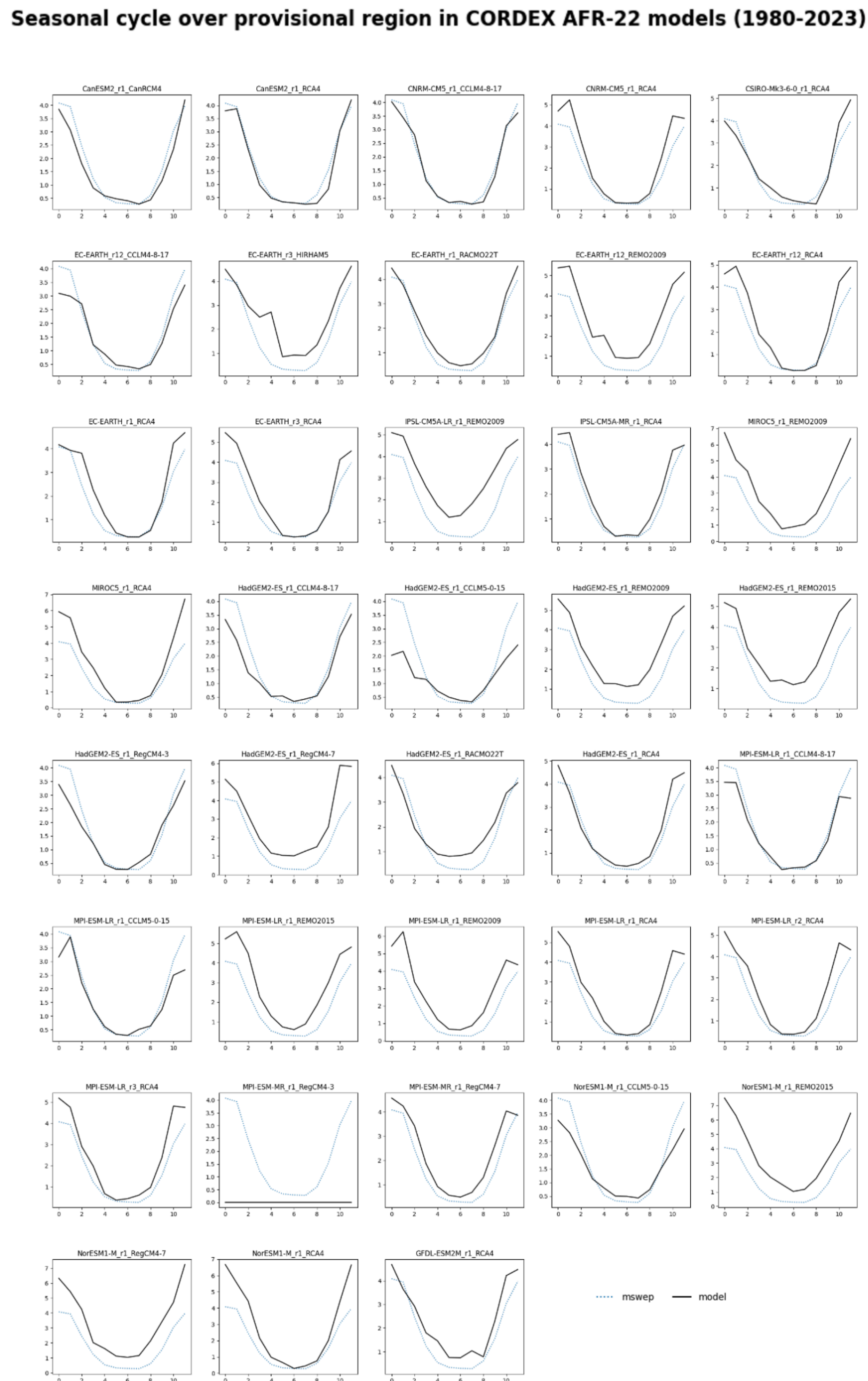

Figure A.2.2: *Seasonal cycles of precipitation in observations shown in blue dotted, and CORDEX models, shown in black.*

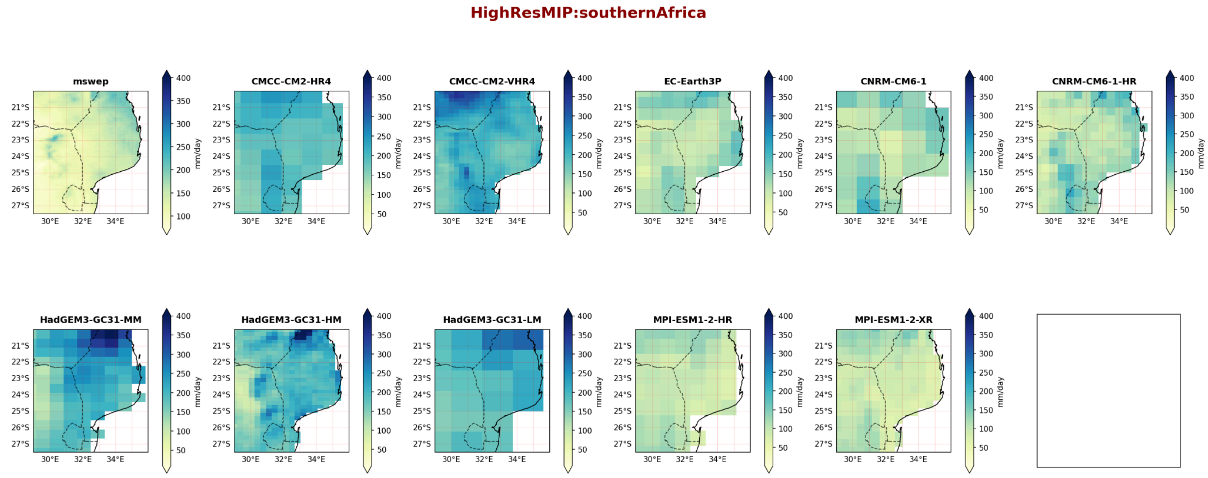

Figure A.2.3: *Spatial patterns of DJF precipitation in observations and HighResMIP models over the study domain.*

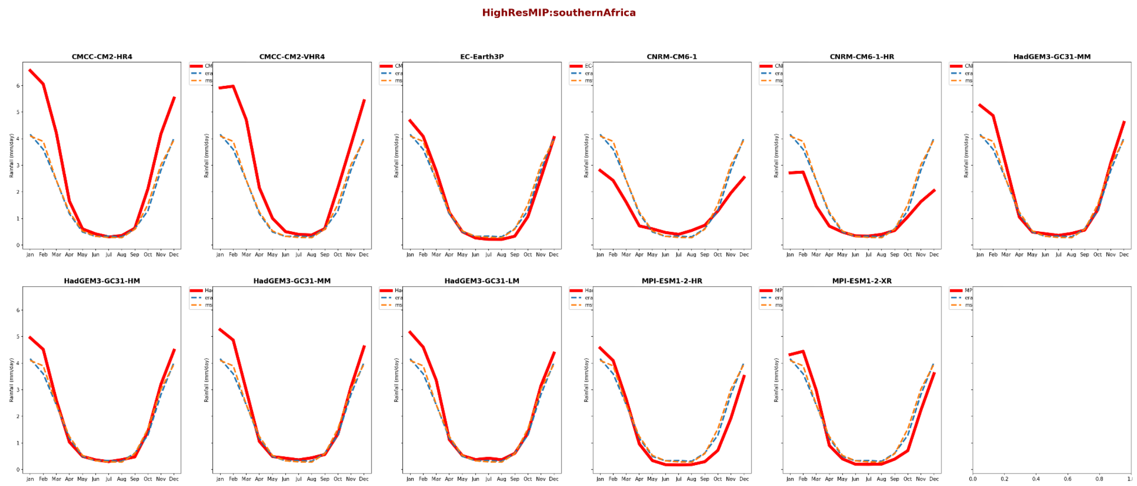

Figure A.2.4: *Seasonal cycles of precipitation in observations shown in dotted blue (ERA5) and dotted orange (MSWEP), and CORDEX models, shown in blue.*

A3 Model evaluation tables

Table A3.1: *Evaluation results of the climate models considered for attribution analysis of VARIABLE. For each model, the threshold for a 1-in-X-year event is shown, along with the best estimates of the Dispersion and Shape parameters are shown, along with a 95% confidence intervals. Furthermore evaluation of the seasonal cycle and spatial pattern are shown.*

Model / Observations	Seasonal cycle	Spatial pattern	Dispersion	Shape parameter	Conclusion
cpc			0.328 (0.240 ... 0.392)	0.019 (-0.20 ... 0.22)	
era5			0.370 (0.300 ... 0.432)	-0.099 (-0.26 ... 0.034)	
mswep			0.357 (0.270 ... 0.417)	0.053 (-0.17 ... 0.30)	

tamsat			0.265 (0.200 ... 0.307)	-0.087 (-0.39 ... 0.17)	
chirps			0.286 (0.216 ... 0.343)	-0.17 (-0.41 ... 0.020)	
CORDEX					
CanESM2_CanRCM4_r1 ()	bad	bad	0.314 (0.145 ... 0.376)	-0.042 (-0.54 ... 0.74)	bad
CanESM2_RCA4_r1 ()	bad	good	0.464 (0.311 ... 0.559)	-0.18 (-0.95 ... 0.60)	bad
CNRM-CM5_CCLM4-8-17_r1 ()	good	reasonable	0.306 (0.177 ... 0.371)	-0.41 (-0.83 ... 0.23)	reasonable (2)
CNRM-CM5_RCA4_r1 ()	reasonable	reasonable	0.342 (0.181 ... 0.424)	0.049 (-0.54 ... 1.6)	reasonable (3)
CSIRO-Mk3-6-0_RCA4_r1 ()	bad	reasonable	0.407 (0.245 ... 0.477)	0.075 (-0.63 ... 0.81)	bad
EC-EARTH_RACMO22T_r1 ()	good	bad	0.221 (0.147 ... 0.271)	-0.39 (-0.75 ... -0.022)	bad
EC-EARTH_RCA4_r1 ()	bad	reasonable	0.342 (0.169 ... 0.396)	0.14 (-0.14 ... 1.3)	bad
EC-EARTH_CCLM4-8-17_r12 ()	good	reasonable	0.335 (0.218 ... 0.417)	-0.0016 (-0.55 ... 0.37)	reasonable (1)
EC-EARTH_RCA4_r12 ()	reasonable	reasonable	0.293 (0.191 ... 0.373)	-0.28 (-0.86 ... -0.043)	reasonable (2)
EC-EARTH_REMO2009_r12 ()	reasonable	reasonable	0.318 (0.202 ... 0.392)	0.019 (-0.39 ... 0.45)	reasonable (3)
EC-EARTH_HIRHAM5_r3 ()	bad	reasonable	0.176 (0.100 ... 0.227)	0.088 (-0.43 ... 0.68)	bad
EC-EARTH_RCA4_r3 ()	reasonable	reasonable	0.354 (0.248 ... 0.427)	-0.23 (-0.65 ... 0.041)	reasonable (2)
GFDL-ESM2M_RCA4_r1 ()	reasonable	reasonable	0.373 (0.227 ... 0.431)	-0.33 (-0.78 ... 0.47)	reasonable (2)
HadGEM2-ES_CCLM4-8-17_r1 ()	good	reasonable	0.400 (0.256 ... 0.451)	-0.73 (-0.98 ... -0.040)	reasonable (2)
HadGEM2-ES_CCLM5-0-15_r1 ()	good	reasonable	0.462 (0.292 ... 0.552)	0.32 (-0.25 ... 0.98)	reasonable (2)
HadGEM2-ES_RACMO22T_r1 ()	good	reasonable	0.267 (0.165 ... 0.329)	0.18 (-0.18 ... 0.65)	reasonable (1)
HadGEM2-ES_RCA4_r1 ()	reasonable	reasonable	0.345 (0.232 ... 0.419)	0.019 (-0.50 ... 0.36)	reasonable (2)
HadGEM2-ES_RegCM4-3_r1 ()	good	bad	4.27 (0.839 ... 8.81)	4.3 (-0.98 ... 4.7)	bad
HadGEM2-ES_RegCM4-7_r1 ()	reasonable	reasonable	0.287 (0.161 ... 0.365)	-0.032 (-0.48 ... 0.30)	reasonable (2)
HadGEM2-ES_REMO2009_r1 ()	reasonable	reasonable	0.277 (0.149 ... 0.331)	0.19 (-0.15 ... 0.92)	reasonable (3)
HadGEM2-ES_REMO2015_r1 ()	reasonable	reasonable	0.248 (0.145 ... 0.311)	0.22 (-0.12 ... 1.0)	reasonable (3)
IPSL-CM5A-LR_REMO2009_r1 ()	reasonable	reasonable	0.284 (0.186 ... 0.337)	-0.14 (-0.64 ... 0.44)	reasonable (3)

IPSL-CM5A-MR_RCA4_r1 ()	good	reasonable	0.407 (0.248 ... 0.495)	0.15 (-0.45 ... 1.3)	reasonable (1)
MIROC5_RCA4_r1 ()	bad	reasonable	0.308 (0.213 ... 0.378)	-0.087 (-0.53 ... 0.55)	bad
MIROC5_REMO2009_r1 ()	reasonable	bad	0.199 (0.128 ... 0.251)	-0.070 (-0.69 ... 0.30)	bad
MPI-ESM-LR_CCLM4-8-17_r1 ()	good	bad	0.362 (0.244 ... 0.435)	0.20 (-0.10 ... 0.64)	bad
MPI-ESM-LR_CCLM5-0-15_r1 ()	good	reasonable	0.397 (0.285 ... 0.464)	0.0055 (-0.62 ... 0.56)	reasonable (1)
MPI-ESM-LR_RCA4_r1 ()	reasonable	reasonable	0.431 (0.292 ... 0.534)	-0.16 (-0.82 ... 0.32)	reasonable (2)
MPI-ESM-LR_REMO2009_r1 ()	reasonable	reasonable	0.398 (0.251 ... 0.504)	-0.050 (-0.35 ... 0.41)	reasonable (2)
MPI-ESM-LR_REMO2015_r1 ()	reasonable	reasonable	0.391 (0.253 ... 0.476)	-0.13 (-0.49 ... 0.40)	reasonable (2)
MPI-ESM-LR_RCA4_r2 ()	reasonable	reasonable	0.389 (0.260 ... 0.490)	-0.16 (-0.62 ... 0.25)	reasonable (2)
MPI-ESM-LR_RCA4_r3 ()	reasonable	reasonable	0.314 (0.207 ... 0.399)	-0.74 (-0.98 ... -0.36)	reasonable (2)
MPI-ESM-MR_RegCM4-7_r1 ()	reasonable	bad	0.436 (0.285 ... 0.521)	0.032 (-0.38 ... 0.67)	bad
NorESM1-M_CCLM5-0-15_r1 ()	good	reasonable	0.348 (0.228 ... 0.425)	0.19 (-0.51 ... 0.70)	reasonable (1)
NorESM1-M_RCA4_r1 ()	reasonable	good	0.256 (0.121 ... 0.332)	0.28 (-0.17 ... 3.8)	reasonable (1)
NorESM1-M_RegCM4-7_r1 ()	reasonable	bad	0.272 (0.184 ... 0.337)	-0.12 (-0.44 ... 0.13)	bad
NorESM1-M_REMO2015_r1 ()	reasonable	good	0.205 (0.0855 ... 0.257)	0.17 (-0.081 ... 1.2)	reasonable (1)
HIGHRESMIP					
CMCC-CM2-HR4 ()	reasonable	good	0.0878 (0.0404 ... 0.115)	-0.36 (-0.65 ... 0.32)	bad
CMCC-CM2-VHR4 ()	reasonable	good	0.0867 (0.0577 ... 0.109)	-0.37 (-0.90 ... -0.021)	bad
CNRM-CM6-1 ()	reasonable	good	0.269 (0.200 ... 0.322)	-0.19 (-0.50 ... 0.14)	reasonable (1)
CNRM-CM6-1-HR ()	reasonable	good	0.252 (0.182 ... 0.307)	-0.33 (-0.64 ... -0.049)	reasonable (1)
EC-Earth3P ()	good	good	0.151 (0.0955 ... 0.185)	-0.49 (-0.77 ... -0.24)	bad
EC-Earth3P-HR ()	good	good	0.0979 (0.0611 ... 0.123)	-0.25 (-0.82 ... 0.057)	bad
HadGEM3-GC31-HM ()	good	good	0.119 (0.0807 ... 0.154)	-0.35 (-0.80 ... 0.082)	bad
HadGEM3-GC31-LM ()	good	good	0.106 (0.0744 ... 0.135)	-0.46 (-0.93 ... -0.19)	bad
HadGEM3-GC31-MM ()	good	good	0.107 (0.0695 ... 0.155)	-0.094 (-0.74 ... 0.44)	bad

MPI-ESM1-2-HR ()	good	good	0.131 (0.0882 ... 0.162)	-0.40 (-0.86 ... -0.21)	bad
MPI-ESM1-2-XR ()	good	good	0.117 (0.0811 ... 0.144)	-0.32 (-0.64 ... 0.048)	bad